INORGANIC CHEMISTRY
FRONTIERS

REVIEW

View Article Online
View Journal | View Issue

Cite this: *Inorg. Chem. Front.*, 2021, **8**, 3587

Turn-on detection of assorted phosphates by luminescent chemosensors

Pramod Kumar, *† Sanya Pachisia and Rajeev Gupta *

This review article presents a variety of luminescent chemosensors for the selective detection of assorted biologically relevant phosphates (phosphate ion, pyrophosphate ion and AMP, ADP and ATP) *via* the "Turn-On" emission mechanism. The focus has been placed to understand the design aspects, chemical structures and luminescence properties including binding constants, detection limits and lifetime parameters of the chemosensors and their emission enhancement based detection mechanism. The article concludes by addressing various future prospects both for the biological and the environmental challenges in front of the scientific community to develop intelligent chemosensors not only for detection purposes but also for remediation processes.

Received 9th January 2021,
Accepted 7th May 2021

DOI: 10.1039/d1qi00032b

rsc.li/frontiers-inorganic

1. Introduction

Phosphate ion and phosphate containing compounds (PPi, AMP, ADP and ATP) play numerous important roles in various biological processes in living organisms.[1–3] Phosphate ion and phosphate containing compounds are not only important nutrients for living organisms but also required for the biosynthesis of adenosine phosphates,[4] nucleic acids,[5,6] phospholipids[7] and proteins.[3,8] Phosphate containing compounds are also known to participate in various metabolic pathways, including energy transfer,[3,9] protein activation[10,11] and amino acid metabolism.[3,11] For example, while adenosine phosphates (AMP, ADP and ATP) play significant roles in metabolic reactions, such as energy realization,[3,9,11] phosphate group-donors[12] and as signalling molecules;[13] the pyrophosphate ion (PPi) is essential both for DNA sequencing[14] and for DNA replication.[15]

In addition to their biological significance, phosphates are also indispensable components of numerous medicinal and pharmaceutical compounds,[16] detergents,[17] fertilizers,[18] personal care products[19] and building and construction materials[20] while play important roles in the chemical and alloy industries.[21] Due to their widespread roles in biology, environment and industry, phosphates are responsible for contaminating the biological and environmental media as well as

Department of Chemistry, University of Delhi, Delhi-110007, India. E-mail: rgupta@chemistry.du.ac.in; Tel: +91-11-27666646, http://people.du.ac.in/~rgupta/

† Present address: Department of Chemistry, Mahamana Malviya College Khekra (Baghpat), C.C.S. University Meerut, India. E-mail: baliyanpk@gmail.com

Pramod Kumar

Pramod Kumar obtained his Ph.D. from I.I.T. Roorkee under the supervision of Prof. Kaushik Ghosh. He did his post-doctoral work at Charles University in Prague (Czech Republic) and at the University of Delhi (India) under the supervision of Prof. Rajeev Gupta. Presently, he is working as an Assistant Professor in Mahamana Malviya College Khekra, Baghpat (under C.C.S. University, Meerut). His research interests include molecular recognition, design of selective chemosensors and developing sensing devices.

Sanya Pachisia

Sanya Pachisia received her M.Sc. degree from the University of Delhi in 2014. She is currently pursuing her Ph.D. in Chemistry at the University of Delhi under the supervision of Professor Rajeev Gupta. Her research interest focuses on the judicious design of metal–organic cages and metal–organic frameworks offering hydrogen bonding based cavities to evaluate their effect on catalysis, sensing and recognition applications.

other habitats including water bodies.[22] As a consequence, the WHO has recommended 0.1 mg L^{-1} as the permissible limit for the phosphate ion in drinking water.[23] Therefore, monitoring of phosphate ion and different phosphate containing compounds is very critical and essential.[24,25] However, it is very challenging to selectively recognize either a phosphate ion or different phosphate containing compounds.[24–26] Such a difficulty is associated with their pH sensitivity and solution dynamics of either a phosphate ion or different phosphate containing compounds.[24,26] For example, phosphate ion can exist in PO_4^{3-}, HPO_4^{2-}, $H_2PO_4^-$ and of course H_3PO_4 forms depending on the solution pH, and all such forms are considerably solvated.[24,26] Other higher phosphates, such as the pyrophosphate ion (PPi) and adenosine phosphates (AMP, ADP and ATP), are not any exception both in terms of their pH sensitivity and solvation energy.[24,26] The abovementioned challenges become more prominent either when the phosphate ion and phosphate containing compounds are present in aqueous media or when dealing with biological samples.[26,27]

Several analytical techniques have been utilized for the detection of phosphate ions and different phosphate containing compounds.[25,26] Such techniques vary from conventional absorption[28] and NMR (^1H and ^{31}P) spectroscopy[29] and electrochemical studies[30–32] (cyclic and square-wave voltammetry) to surface-based methods[26,33] (electron microscopy including SEM and TEM) to X-ray diffraction methods[34] (powder and single crystal) to isothermal titration calorimetry (ITC), which provides quantitative information including enthalpy, entropy and free energy values for a binding event.[26,35] However, many such techniques suffer from various disadvantages including detailed instrumentation, sample preparation, only provisions for the solid-sample analysis and the requirement of dried samples that may not correctly represent the actual solution-based species.[26] In this context, fluorescence spectroscopy based detection methods are often considered superior due to their high selectivity and sensitivity as well as fast and easy operation.[36,37] Moreover, fluorescent spectral techniques are particularly convenient for cell imaging work and when dealing with biological samples.[38]

Rajeev Gupta

Rajeev Gupta is Professor of Chemistry at the University of Delhi (India). His research group works on several aspects of coordination and supramolecular chemistry with emphasis on architectural aspects, designer materials, catalysis, sensing, and energy-transfer. His research is well-supported by generous funding from SERB, DST, CSIR, DST-PURSE, and UGC. More details about Rajeev Gupta's research work can be found on his website: http://people.du.ac.in/~rgupta/.

Designing a chemosensor for the selective detection of a phosphate ion or various phosphate containing compounds is a challenging task as it requires linking a fluorophore with a receptor with the potential of recognizing an analyte while overcoming pH and solvation related issues.[24,26] Despite such challenges, there has been tremendous advancement in the synthesis of assorted chemosensors which utilize various non-covalent interactions including hydrogen bonding, halogen bonding, and anion···π and π···π interactions for selective binding and therefore sensing of a phosphate ion or various phosphate containing compounds.[26,36,37] Consequently, both organic compound based and metal complex based chemosensors have been developed and exploited for the recognition and binding of various phosphates.[24,26,36,37] The present review article aims to apprise readers about the chemical diversities of various chemosensors and their mode of interaction that is responsible for a detection event. Efforts have also been made to include crystallographic structures,‡ wherever possible, in order to highlight the mode and/or place of interaction between a chemosensor and an analyte.

2. Scope

This review article presents assorted luminescent chemosensors that have been developed for the "Turn-On" emission based detection of different phosphate ions and related phosphate containing compounds. However, this review article has excluded (i) non-luminescent chemosensors; (ii) emission turn-off chemosensors; and (iii) sequestration based chemosensors for the removal of chelated metal ion(s) by using assorted phosphates and related compounds.

The present review article has been divided into two major categories: (i) organic molecule based chemosensors and (ii) metal complex based chemosensors whereas sub-categories have been created based on the nature of the analyte – monophosphates, di-phosphates and adenosine phosphates. While this article is aimed to showcase the chemical diversities of assorted chemosensors and their mode of interaction with phosphates, binding information and crystallographic data wherever available have also been included to illustrate the interaction between a chemosensor and an analyte.

3. Organic molecule based chemosensors

In this section, detection of assorted phosphates utilizing organic molecule based chemosensors, showing "Turn-On" emission properties, has been discussed.

‡In the crystal structure drawings, chemosensors are shown in deep green colour whereas counter anions and lattice solvent molecules have been omitted for clarity. The following colour codes have been used: metal atom, orange; nitrogen atom, blue; oxygen atom, red; phosphorus atom, pink; hydrogen atom, grey.

3.1. Detection of mono-phosphates (PO_4^{3-}, HPO_4^{2-}, and $H_2PO_4^-$)

This section has summarized assorted fluorescent chemosensors used for the 'Turn-On' detection of mono-phosphates such as PO_4^{3-}, HPO_4^{2-} and $H_2PO_4^-$. Kim and co-workers[39] have developed a multifunctional hydroxyjulolidine based chemosensor **1** for the fluorescence detection of PO_4^{3-} ions (Fig. 1a). Interestingly, the presence of phosphate ions led to a significant emission enhancement in a buffer/DMSO mixture (7/3, v/v, pH = 7.0). In comparison with other competing anions, the presence of PO_4^{3-} ions manifested a strong fluorescence at 487 nm (λ_{ex} = 426 nm) to otherwise non-emissive **1**. Absorption spectral studies revealed a 1 : 1 binding stoichiometry between **1** and PO_4^{3-} ions while emission spectral titration yielded a binding constant of 5.7×10^2 M^{-1}. Enhancement in the emission intensity of chemosensor **1** was related to the deprotonation of the phenolic–OH group (**1A**), as suggested by the experimental results and theoretical calculations. In addition to phosphate ions, chemosensor **1** was also found to detect Cu^{2+} and S^{2-} ions.

A cationic tetraphenylethylene dimethylformamidine derivative based chemosensor **2** was developed for the detection of PO_4^{3-} ions (Fig. 1b).[40] The dihydrogen chloride salt of **2** was soluble in water but was non-emissive. Notably, on addition of PO_4^{3-} ions, non-emissive **2** showed an excellent fluorescence at 502 nm (λ_{ex} = 368 nm) in aqueous medium. Importantly, other anions as well as alkali metals and alkali earth metals did not interfere in the emission behaviour of **2**. UV–Vis spectral titration inferred a 1 : 1 stoichiometry between **2** and PO_4^{3-} ions with a binding constant of 2.36×10^4 M^{-1}. Authors showed that only one equivalent of PO_4^{3-} ions transformed non-emissive **2** to its emissive derivative **2A** and HPO_4^{2-} through aggregation-induced emission (AIE).[41] Interestingly, **2A** and HPO_4^{2-} ions formed an aggregate due to the low solubility of **2A** in water and such a fact resulted in emission enhancement through the AIE phenomenon. The presence of one free dimethyl–formamidine unit in **2A**, where imine double bonds and phenyl rings were in conjugation, was responsible to increase the conjugation and thus emission enhancement. However, due to the absence of such a conjugation, chemosensor **2** was non-emissive. The presence of an acid was found to reversibly transform **2A** into **2**.

Wu and co-workers[42] have reported a tetraphenylethene (TPE) based tripodal tris-urea chemosensor **3** for the selective detection of PO_4^{3-} ions (Fig. 2a). In the presence of PO_4^{3-} ions, **3** showed a 20-fold fluorescence enhancement in DMSO. Both experimental and computational studies revealed strong H-bonding between **3** and PO_4^{3-} ions with a 2 : 1 stoichiometry thus forming a capsular assembly. 'Turn-On' behaviour was attributed to strong interaction of PO_4^{3-} ions with **3** which restricted the rotation of the terminal TPE units. Other mono-phosphates, such as HPO_4^{2-} and $H_2PO_4^-$ ions, although inducing significant changes in the NMR spectra of **3** exhibited very weak fluorescence and rather formed 1 : 1 based half-capsules. The crystal structure of chemosensor **3** displayed a tripodal cavity which exhibited both intramolecular and intermolecular N–H···O H-bonds, leading to a 1D assembly. Such a fact was the probable reason for the AIE effect displayed by **3**. On the other hand, H-bonding based half-capsular self-assembly between the HPO_4^{2-} ion and **3** *via* three urea units was confirmed by X-ray crystallography wherein HPO_4^{2-} ions were bound *via* seven N–H···O H-bonds of the three urea arms present in **3** (Fig. 2b). In contrast, DFT studies of **3**·orthophosphate revealed the formation of 12 strong N–H···O H-bonds in addition to CH···π interactions between the adjacent TPE moieties which restricted their movement and caused emission enhancement. Interestingly, docking studies of **3** with PO_4^{3-} ions supported the DFT studies in which N–H protons were involved in H-bonding with the phosphate ion (Fig. 2c).

Zhang and co-workers[43] have reported crystallographically characterized chemosensor **4** for the highly selective sensing

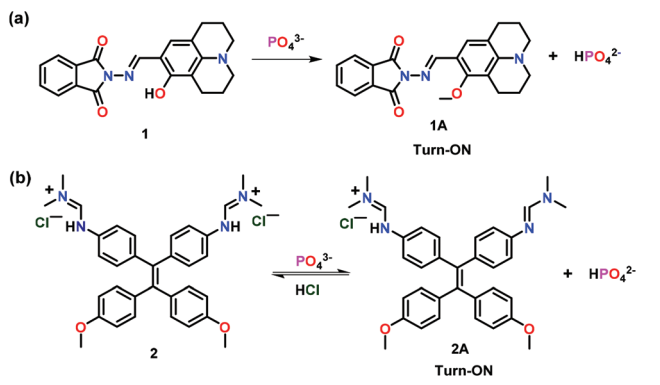

Fig. 1 Chemical drawings of chemosensors (a) **1** and (b) **2** and their proposed 'Turn-On' emission mechanism with PO_4^{3-} ions. Adapted from ref. 39 and 40.

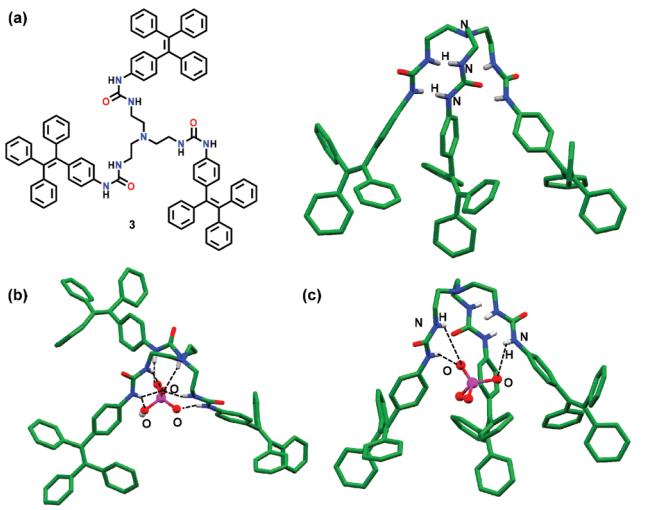

Fig. 2 (a) Chemical drawing and crystal structure of chemosensor **3**; (b) crystal structure depicting inclusion of the monohydrogen phosphate ion (HPO_4^{2-}) within the cavity of **3**; (c) molecular docking of **3** with the PO_4^{3-} ion. Hydrogen atoms except for N–H groups have been omitted clarity. Adapted from ref. 42.

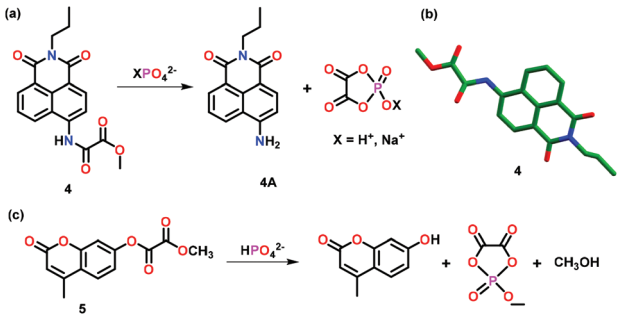

Fig. 3 (a) Chemical drawing of chemosensor **4** and its proposed 'Turn-On' emission mechanism with XPO_4^{2-} ion (X = H^+ or Na^+). (b) Crystal structure of the chemosensor **4**. (c) Chemical drawing of chemosensor **5** and its 'Turn-On' emission mechanism with HPO_4^{2-} ions. Adapted from ref. 43 and 44.

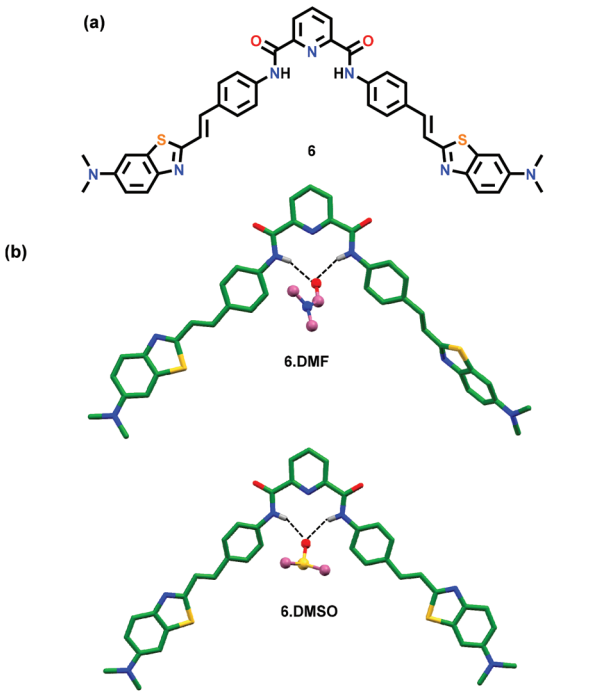

Fig. 4 (a) Chemical drawing of chemosensor **6**. (b) Crystal structures of **6**·DMF and **6**·DMSO displaying H-bonds between a solvent molecule (DMF or DMSO) and amidic N–H groups; other hydrogen atoms have been excluded for clarity. Adapted from ref. 45.

of XPO_4^{2-} ions (X = H^+ or Na^+) over other phosphates such as PPi and ATP both exogenously and endogenously (Fig. 3a–b). Chemosensor **4** exhibited 91-fold fluorescence enhancement accompanied by a 79 nm red-shift in the presence of XPO_4^{2-} ions. These spectral changes could be appreciably correlated with a color change from colorless to light yellow. Importantly, the presence of phosphate ions triggered amide bond cleavage in **4** causing the fluorophore to release, thus, inducing a distinct photo-physical change. Theoretical studies including quantum-mechanical calculations and TDFT aided in elucidating the high selectivity of **4** towards phosphate ions over PPi and other higher structural analogues. In hemichannel-closed Sf9 cells, **4** was able to trace both the generation and accumulation of XPO_4^{2-} ions *via* the fluorescent spectral changes.

Zhou and co-workers[44] have reported a colorimetric and fluorescent chemosensor **5** for the detection of HPO_4^{2-} ions in DMSO–HEPES buffer (v/v = 9 : 1; pH 7.4) (Fig. 3c). Chemosensor **5** undergoes a unique HPO_4^{2-} ion induced hydrolytic reaction that produces a colorimetric change associated with a 62 nm red-shift in the UV–Vis spectrum and a 780-fold enhancement in the emission intensity. Theoretical calculations supported the ester bond hydrolysis for the reaction of **5** with HPO_4^{2-} ions which was further confirmed by the observation of a peak at *m*/*z* 151.08 in the mass spectrum corresponding to the cyclic phosphate. Chemosensor **5** was used for localizing exogenous and endogenous phosphate ions in HeLa cells and *C. elegans* as observed by fluorescence imaging. It was also used to monitor *in vivo* phosphate ion production due to apyrase catalyzed ATP hydrolysis. The *in vitro* phosphate ion release was utilized to elucidate the mechanism of Inx3 action in hemichannel-closed Sf9 cells.

Rurack and co-workers[45] have reported a pyridine-2,6-dicarboxamide based chemosensor **6** containing two styryl chromophores (Fig. 4a). Chemosensor **6** exhibited an emission output between 500 and 600 nm which further increased in the presence of $H_2PO_4^-$ ions due to the formation of intramolecular H-bonds in the resultant host–guest ensemble. The formation of intramolecular H-bonds was confirmed by the crystal structure analysis of **6**·DMF and **6**·DMSO which assisted in understanding the sensing mechanism and the generation of the actual species responsible for the emission enhancement (Fig. 4b). A solvent molecule was found to create H-bonds through its O-atom with the amidic N–H groups. The chemosensor existed in an unusual conformation where one of its styryl groups was coplanar along with the pyridine-2,6-dicarboxamide unit whereas the second one was at a slightly tilted angle which allowed either a solvent molecule or a guest to reside within the cavity and form both inter- and intra-molecular H-bonds.

Ghosh and co-workers[46] have reported a series of anthracene appended bis-amide based chemosensors **7**–**10** bearing different spacers (Fig. 5). All four chemosensors exhibited significant 'Turn-On' fluorescent sensing for the $H_2PO_4^-$ ion in CH_3CN. The sensing ability of such chemosensors was highly dependent on the type of spacer between the amide groups. During the binding with the $H_2PO_4^-$ ion, monomer emissions of **7**–**10** were little perturbed while the excimer emissions at *ca.* 500 nm were amplified due to the closeness of the anthracene moieties. The excimer emission of **8** was found to increase many-fold as compared to **7**. This was presumably due to the fewer conformational changes of **8** containing a picolinamide spacer than that of **7** bearing an isophthalamide spacer. In the case of **9** and **10**, glutaroyl and adipoyl spacers introduced greater flexibility and thus repositioning of the anthracenyl groups becomes much easier. Hence, excimer emission was enhanced for chemosensors **9** and **10** in the presence of $H_2PO_4^-$ ions. Interestingly, excimer growth in **10** (with a flex-

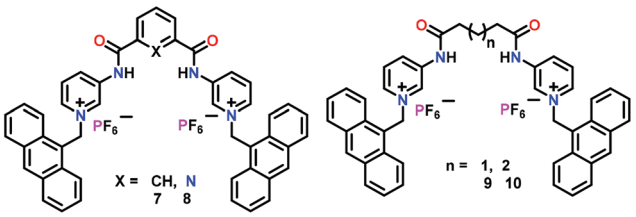

Fig. 5 Chemical drawings of chemosensors **7–10**. Adapted from ref. 46.

ible spacer) was significantly greater than in **7**. Due to the significant binding of $H_2PO_4^-$ ions, these chemosensors were used for cell staining and DNA interaction studies. This was also one of the first examples where amide-based receptors exhibited significant interaction with DNA.

Molina and co-workers[47] have developed BINOL-based chiral chemosensors (**11–14**) bearing triazolium linked ferrocenyl or phenyl groups (Fig. 6). These chemosensors functioned based on the anion···anion interactions for the detection of $H_2PO_4^-$ ions. NMR spectral studies indicated selective interaction of these cationic receptors with $HP_2O_7^{3-}$ and $H_2PO_4^-$ ions through non-covalent interactions. However, optical studies confirmed that only $H_2PO_4^-$ ions exhibited changes in absorption and fluorescence spectra in CH_3CN. As expected, **14** showed very weak emission due to the presence of bulkier ferrocene and iodide groups and the emission was not restored after the addition of any phosphate. On the other hand, **11** showed little enhancement for monomer emission at 365 nm along with a new excimer emission at 465 nm with $H_2PO_4^-$ ions. **11** also worked as the "naked eye" fluorescent detector for $H_2PO_4^-$ ions in CH_3CN. Chemosensor **12** showed weak emission bands at 359, 374, and 390 nm in CH_3CN but exhibited significant enhancement with $H_2PO_4^-$ ions. Likewise, **13** exhibited similar sensing behaviour as noted for **12** with 30-fold quantum yield related to the free chemosensor. The crystal structure of **11** with PPi confirmed the existence of H-bonding interactions where C–H units of the triazolyl moiety behaved as the H-bond donor to the H-bond acceptor anion $H_2P_2O_7^{2-}$ (Fig. 6b).

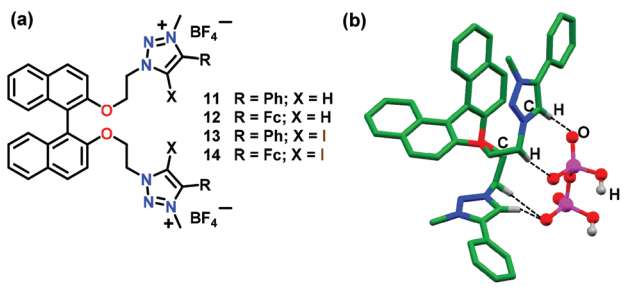

Fig. 6 (a) Chemical drawings of chemosensors **11–14**. (b) Crystal structure of **11**·$H_2P_2O_7^{2-}$ depicting H-bonding between the host and $H_2P_2O_7^{2-}$ ion. Hydrogen atoms, except for those involved in H-bonding interactions, have been omitted for clarity. Adapted from ref. 47.

Molina and co-workers[48,49] have developed imidazolium-based chemosensors **15–17** containing 2,7-disubstituted naphthalene while containing appended anthracene groups as the fluorophores (Fig. 7). The three chemosensors exhibited characteristic bands at 396, 418 and 442 nm for the anthracene moiety in CH_3CN (λ_{ex} = 370 nm). The Br-substituted **15** worked as a selective chemosensor for the $H_2PO_4^-$ ion and promoted excimer formation of anthracene (at 465 nm) with a concomitant quenching of the monomer emission bands. Chemosensor **15** however showed quenching in the presence of F^-, SO_4^{2-} and $HP_2O_7^{3-}$ anions. Interestingly, addition of $HP_2O_7^{3-}$ ions to **15** showed two different concentration effects; addition of up to 1 equiv. exhibited a weak enhancement of excimer emission and quenching of the monomer emission bands. However, further addition of $HP_2O_7^{3-}$ ions only enhanced the monomer emission bands. Chemosensor **16** also showed quenching of the monomer emission bands in the presence of phosphates, F^- and SO_4^{2-} ions. Similar to **15**, **17** showed nearly identical behaviour both towards $H_2PO_4^-$ and $HP_2O_7^{3-}$ ions. In the presence of $H_2PO_4^-$ ions, **17** also showed a remarkable quenching of the monomer emission bands and a progressive formation of the anthracene excimer band. With $HP_2O_7^{3-}$ ions, **17** showed two unlike effects: addition of up to 1.8 equiv. induced an enhancement of the monomer emission bands while further addition of more than 1.8 equiv. promoted a continuous quenching of the monomer emission band. Experiments with HeLa cells proved that **15** showed very good cell membrane permeability and therefore could be used as an efficient imaging agent in living cells.

3.2. Detection of di-phosphates (pyrophosphate ion (PPi) and its derivatives)

In this section, organic molecule based chemosensors have been summarized, which were utilised for the 'Turn-On' detection of the pyrophosphate ion (PPi) and its derivatives.

Sessler and co-workers[50] have developed an excimer disaggregation induced emission (EDIE) method[51] for the detection of pyrophosphate and phosphate ions. The dipositively charged macrocycle **18** containing pyridyl-imidazolium groups was found to exhibit a supramolecular polymer in the solid state as established by crystallography (Fig. 8). The presence of pyridine rings, cationic imidazolium and phenylene groups

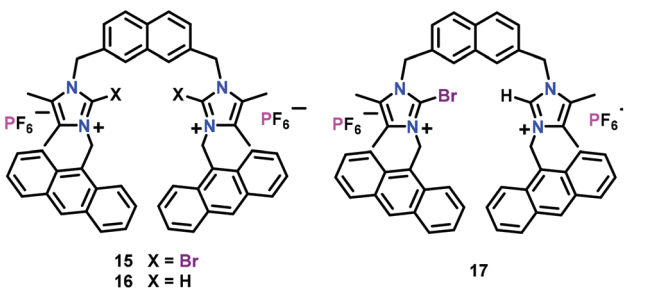

Fig. 7 Chemical drawings of chemosensors **15–17**. Adapted from ref. 48 and 49.

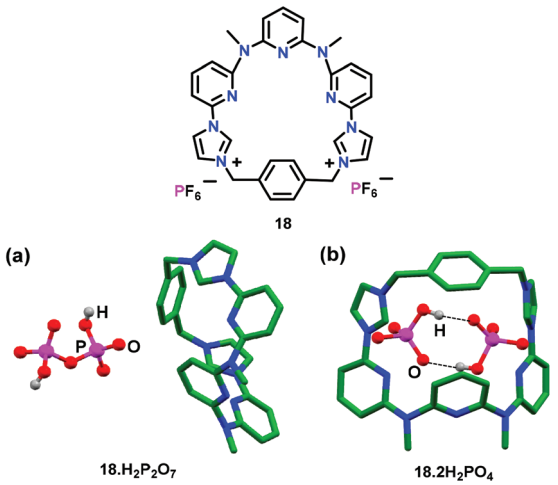

Fig. 8 Chemical drawing of chemosensor **18**. Crystal structures of (a) **18**·$H_2P_2O_7$ and (b) **18**·$2H_2PO_4$. Hydrogen atoms except for phosphate anions have been excluded for clarity. Adapted from ref. 50.

made **18** behave as a potential intermolecular H-bond acceptor as well as donor. Interestingly, **18** showed a concentration-dependent fluorescence at 415 nm (λ_{ex} = 334 nm) and exhibited emission enhancement up to 0.02 mM concentration in CH_3CN. On further increase, concomitant formation of an excimer (*ca.* 500 nm) was noted due to the self-association led aggregation. Macrocycle **18** showed a 200-fold emission enhancement with $HP_2O_7^{3-}$ ions as compared to other oxo-anions and anions. Turn-on fluorescence was also observed with $H_2PO_4^-$ and HCO_3^- ions but to a lesser extent. Turn-on detection of $HP_2O_7^{3-}$ ions occurred due to the dis-aggregation of non-fluorescent excimers to generate monomers with strong emission. The formation of a fluorescent H : G complex with $HP_2O_7^{3-}$ (1 : 1) and $H_2PO_4^-$ (1 : 2) diminished the strong interactions in excimer formation, as confirmed by the crystallographic studies (Fig. 8b). Single crystal analysis of **18** with pyrophosphate ions exhibited a sitting-top anion-complex which minimized the interaction of macrocycles with each other and hence induced an enhancement in the fluorescence intensity due to the dis-aggregation of the excimer. The crystal structure of **18**·$2H_2PO_4$ exhibited a similar stoichiometry as noted in the solution state (Fig. 8b). Herein, two $H_2PO_4^-$ anions existed together stabilized by H-bonds between them. The structure was further stabilized by the occurrence of both anion···π interactions and H-bonds formed between charged (imidazolium rings) and neutral (benzene ring) C–H groups to that of anion–O atoms.

Sessler and co-workers[52] have reported a calix[4]pyrrole based receptor **19** (Fig. 9a) for the detection of PPi using indicator displacement assay (IDA).[53] For this purpose, tetrabutylammonium-2-oxo-4-(trifluoromethyl)-2*H*-chromen 7-olate (chromenolate ion) was utilized, which formed a non-emissive complex with **19**. After the addition of the pyrophosphate ion (PPi) into CH_3CN, a non-emissive complex showed an enhanced emission at 500 nm due to the replacement of the

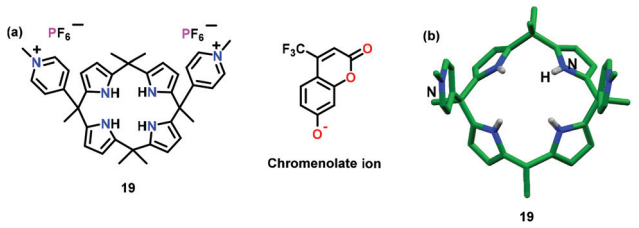

Fig. 9 Chemical drawing (a) and crystal structure (b) of chemosensor **19**. Adapted from ref. 52.

chromenolate ion. A similar fluorescence change was observed in aqueous medium. The binding constant ($K_b \times 10^6$ M^{-1}) for the detection of PPi by **19** was 25.5 in CH_3CN and 3.63 in 30% water–CH_3CN mixture. A combination of H-bonding, anion···π and electrostatic interactions was responsible for the detection of pyrophosphate ions, which was also supported by the crystal structure of free **19** (Fig. 9b).

Molina and co-workers[54] have developed a series of dicationic triazolium–pyrene based receptors **20–23** (Fig. 10). In these chemosensors, detection of pyrophosphate ions was triggered by the operation of only H-bonds (**20**), only halogen-(X)-bonds (**21** and **22**) and a combination of both H- and X-bonding interactions (**23**). These chemosensors showed a dramatic fluorescent enhancement of the excimer band at 473 nm (λ_{ex} = 340 nm) in the presence of only $HP_2O_7^{3-}$ ions as compared to other anions. It was found that only hydrogen pyrophosphate formed X-bonding complexes with these receptors and the association constants were in the order of $\approx 10^6$ M^{-1} while detection limits were of order $\approx 10^{-7}$ M. A 1 : 1 stoichiometry was calculated *via* ^{1}H NMR spectral titrations of chemosensors **20–23** with $HP_2O_7^{3-}$ ions. NMR spectral titrations and computational studies suggested that in comparison with the H-bonded analogue, X-bonded complexes increased the strength of hydrogen pyrophosphate binding.

Ghosh and co-workers[55] have reported benzimidazolium-based receptors **24** and **25** with identical binding sites, while bearing different fluorophores (Fig. 11). Both receptors displayed different sensing behaviour under identical conditions for different phosphates. At lower concentration of phosphates, emission enhancement was observed for $HP_2O_7^{3-}$ and $H_2PO_4^-$ ions by **24** and **25**, respectively. The sensing difference

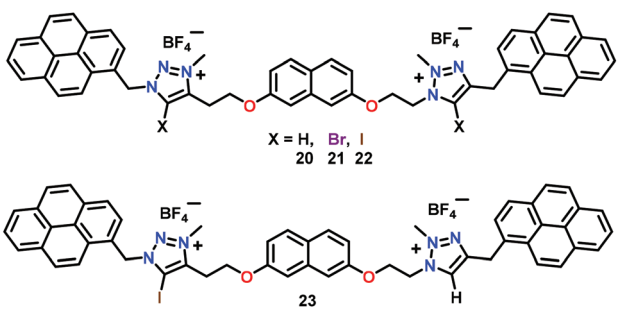

Fig. 10 Chemical drawings of chemosensors **20–23**. Adapted from ref. 54.

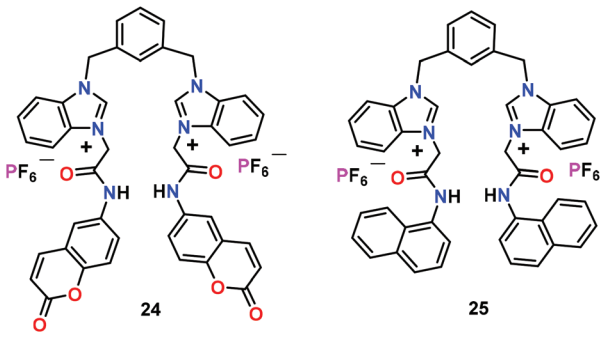

Fig. 11 Chemical drawings of chemosensors **24** and **25**. Adapted from ref. 55.

between **24** and **25** was due to the position of the fluorophores which optimized the binding cavity size of a receptor. At higher concentration of anions, **24** revealed selectivity in the sensing of $HP_2O_7^{3-}$ and $H_2PO_4^-$ ions in CH_3CN. However, **25** only detected F^- ions under identical conditions. It was noted that F^- ions exhibited strong affinity with amide and benzimidazolium groups of **24**. Interestingly, both chemosensors **24** and **25** formed supramolecular gels with $HP_2O_7^{3-}$ and $H_2PO_4^-$ ions, respectively. The gel formation ratified visual sensing of $HP_2O_7^{3-}$ and $H_2PO_4^-$ ions as other anions were unsuccessful. Authors reasoned that gelation of **24** and **25** took place due to the intermolecular chelation of the benzimidazolium-based receptors to the anion wherein solvent molecules were entrapped. In aqueous CH_3CN (1 : 1; v/v), chemosensor **25** showed moderate selectivity for ATP while **24** did not show any selectivity for any phosphate. Experimental results and DFT calculations showed that the different cavity size of **24** and **25**, due to different fluorophores around the binding sites as well as the involvement of fluorophores–protons in the interaction with anions, was responsible for anion selectivity.

Ghosh and co-workers[56] have used a positively charged pyridinium-functionalized chemosensor **26** for the selective detection of $HP_2O_7^{3-}$ ions in both CH_3CN and CH_3CN/Tris-HCl buffer (4 : 1 v/v, pH = 6.5) (Fig. 12). Chemosensor **26** illustrated a new excimer emission peak at 520 nm with $HP_2O_7^{3-}$ ions in CH_3CN. However, in aqueous–CH_3CN, monomer emission (412 nm) considerably increased without any peak corresponding to the excimer/exciplex. The binding constant for the interaction of **26** with $HP_2O_7^{3-}$ ions in CH_3CN/H_2O was 9.59×10^4 M^{-1} while the stoichiometry was 1 : 1. For practical application, they connected receptor **26** with a resin support. The resultant resin-beads (*i.e.*, **27**) efficiently sensed $HP_2O_7^{3-}$ ions in CH_3CN/H_2O (4 : 1 v/v) and pure aqueous medium at pH 6.5. In addition, both chemosensor **26** and its polymeric version **27** were used in the Indicator Displacement Assay (IDA) technique[53] using uranine dye to support naked-eye detection of the $HP_2O_7^{3-}$ ion. A combination of H-bonding, electrostatic interactions and the cleft size controlled the selective recognition of the guest. The blood serum experiments suggested that the resin-bead based **27** can also detect $HP_2O_7^{3-}$ ions in the biological systems.

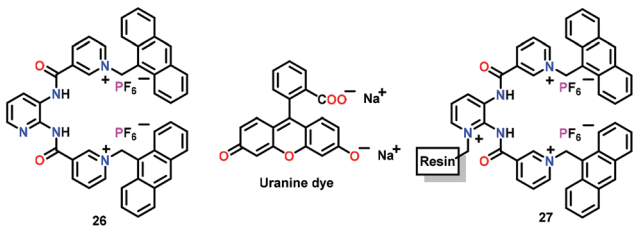

Fig. 12 Chemical drawings of chemosensors **26** and **27**. Adapted from ref. 56.

3.3. Detection of adenosine phosphates (AMP, ADP and ATP)

This section has summarized organic molecule based chemosensors for the 'Turn-On' detection of various adenosine phosphates such as AMP, ADP and ATP.

Tan and co-workers[57] have reported a rhodamine based chemosensor **28** containing a diethylenetriamine unit for anion binding and a triphenylphosphonium unit for mitochondrion targeting (Fig. 13). Chemosensor **28** was used for the selective recognition of ATP in mitochondria. In the presence of ATP (PBS, pH = 7.4), a non-emissive spirolactam form of **28** exhibited intense fluorescence at 583 nm (λ_{ex} = 520 nm), manifesting that the spirolactam ring is in open conformation. The sequential addition of ATP progressively raised the fluorescence of **28** while reaching 81-fold at 10 mM ATP concentration. The spirolactam ring-opening produced a naked-eye colour change from colourless to pink with a detection limit of 0.033 mM. The ATP detection was due to the diethylenetriamine unit which interacted with the phosphate groups of ATP whereas π···π stacking between the adenine ring of ATP and xanthene moiety of rhodamine also contributed. The spectral titration showed a 1 : 1 stoichiometry of **28** with ATP with

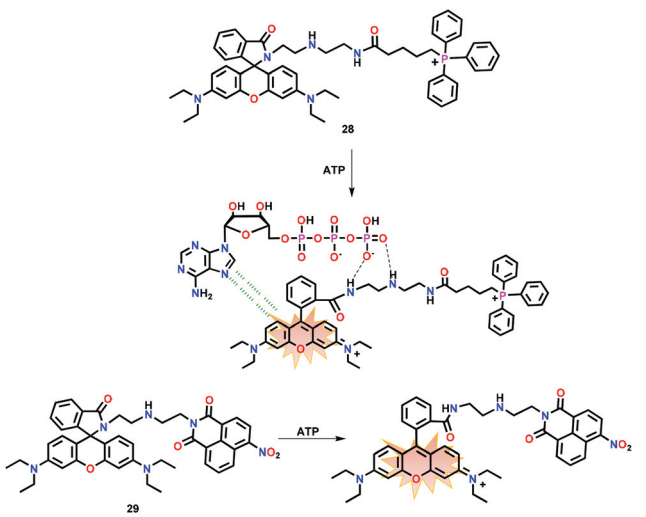

Fig. 13 Chemical drawings of chemosensors **28** and **29** and their proposed binding with ATP through π···π interactions with the open conformation of the spirolactum ring. Adapted from ref. 57 and 58.

K_b of 215.6 M^{-1}. The pH dependent fluorescence displayed an appreciable response towards ATP within the pH range of 6.0–8.0 which created the possibility for the detection of ATP in biological media. Notably, **28** was also used for monitoring and the recognition of mitochondrial ATP concentration in HeLa cells.

Ma and co-workers[58] have also reported a rhodamine-based chemosensor **29** for the detection of ATP in TRIS buffer at pH 7.4 (Fig. 13). In the presence of ATP, chemosensor **29** showed 110-fold 'Turn-On' emission at 580 nm (λ_{ex} = 540 nm). The emission enhancement was observed as a result of spirolactam ring-opening involving π···π stacking and multiple H-bonding interactions. Chemosensor **29** was also used for ATP monitoring in live cells.

Yuan and co-workers[59] have developed a reversible fluorescent chemosensor **30** for the quantitative detection and real-time monitoring of mitochondrial ATP in the living cells (Fig. 14). The chemosensor **30** showed a weak yellow fluorescence at 560 nm and a red fluorescence at 624 nm due to the photo-induced electron transfer (PET) in HEPES buffer (containing 10% EtOH; pH 7.4; λ_{ex} = 500 nm). Upon addition of ATP, the PET process was blocked while a six-fold enhancement in the intensity ratio (F_{624}/F_{560}) was observed. Chemosensor **30** selectively and reversibly responded to ATP with a dissociation constant of 4.65 mM. Notably, **30** was used for the monitoring of mitochondrial ATP in the normal and the cancer cell lines.

Anzenbacher Jr. and co-workers[60] have reported an anthracene functionalized chemosensor **31** bearing two imidazolium hydrazone groups for ATP detection in water (Fig. 15). Chemosensor **31** is non-fluorescent in aqueous medium; however, it exhibited a bright green coloured 35-fold 'Turn-On' emission at 504 nm in the presence of ATP. In contrast, only 8-fold 'Turn-On' emission was perceived in the presence of ADP. Emission spectral titrations yielded binding constants ($K_b \times 10^2$ M^{-1}) of 13.0 and 1.0 for ATP and ADP, respectively. The 1 : 1 binding stoichiometry was noted for ATP using Job's plot. The excellent selectivity of **31** towards ATP was the result of combined effects of π···π interactions between the adenine ring of ATP and anthracene unit of the chemosensor as well as electrostatic interactions between the oppositely charged phosphates and imidazolium groups of **31**.

Cao and co-workers[61] have used related tetraphenylethene (TPE) based AIE chemosensors **32–36** for the recognition of ATP in aqueous medium (Fig. 16). In these chemosensors, two TPE moieties were connected to a bis-imidazolium core separated with different methylene spacers. All five chemosensors revealed weak fluorescence in aqueous solution; however, a significant emission enhancement was observed with ATP at 471 nm (λ_{ex} = 365 nm) in a THF–water mixture due to TPE-based aggregation. Notably, binding affinity of chemosensors **32–36** towards ATP could be tuned with the aid of the spacer length, wherein, binding constants varied in the following order: **32** > **33** > **34** > **35** > **36** (11.9×10^4 to 1.46×10^4 M^{-1}). Detection limits were found to be in the range of 4.15 to 16.8 nm. The dynamic light scattering (DLS) and ^{1}H NMR spectral titrations explained the vital role of two imidazolium units in binding with the anionic triphosphate group of ATP. Such interactions were found to enhance the aggregation of chemosensors by decreasing the solubility and as a result exhibited an AIE-based 'Turn-On' emission.[41] Importantly, binding affinity towards ATP and the chain length of two charged imidazolium units could be directly correlated. In fact, chemosensors with shorter linkers matched with the size of the phosphate anion of ATP, thus yielding a higher binding towards ATP.

Ma and co-workers[62] have reported cationic chemosensors **37–39** containing pyridinium functionalized boronic acid groups for the AIE based[41] selective recognition of ATP (Fig. 17). These chemosensors recognized ATP through AIE in a H_2O–DMSO mixture at pH = 7. All three chemosensors exhibited emission enhancement with ATP. Among these receptors, the tripodal one (**39**) showed a better selectivity and sensitivity towards ATP with a detection limit of 0.3 ppm. The strong affinity of **39** with ATP was due to the presence of both

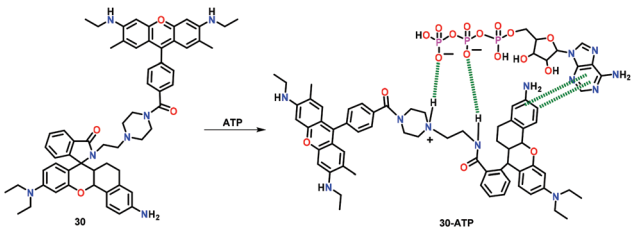

Fig. 14 Chemical drawing of chemosensor **30** and its proposed binding with ATP. Adapted from ref. 59.

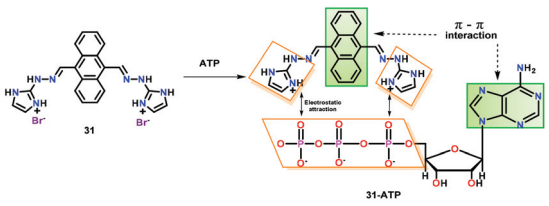

Fig. 15 Chemical drawing of chemosensor **31** and its proposed binding with ATP through π···π interactions and electrostatic attraction. Adapted from ref. 60.

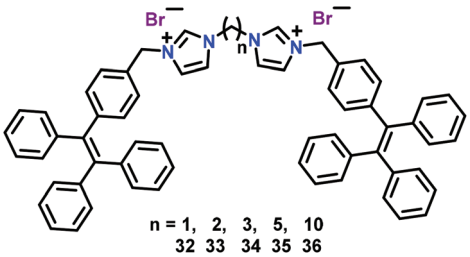

Fig. 16 Chemical drawings of chemosensors **32–36**. Adapted from ref. 61.

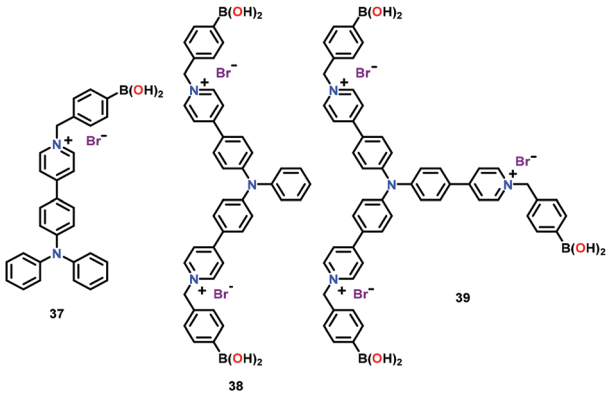

Fig. 17 Chemical drawings of chemosensors **37–39**. Adapted from ref. 62.

electrostatic and covalent bonding interactions involving pyridinium and boronic acid groups, respectively. Authors concluded that the chemosensors with multiple binding sites were capable of detecting ATP efficiently from a pool of other anions. The penetrating power into cells, specifically nucleus, depended on the quantity of positive charges as well as the boronic acid groups in these chemosensors.

Ghosh and co-workers[63] have developed a tripodal receptor **40** containing pyridinium units linked with the appended naphthyl groups (Fig. 18). Chemosensor **40** showed emission at 386 nm (λ_{ex} = 290 nm) in CH_3CN/HEPES buffer (1 : 1, v/v, pH = 6.5). Upon interaction with biologically relevant phosphates, the emission enhancement was observed at 390 nm for ATP over ADP and AMP. The emission peak at 390 nm was due to the exciplex formation between the naphthalene moieties of **40** and adenine unit of ATP. The binding constant and detection limit for ATP were found to be 1.16 × 10^3 M^{-1} and 8.44 μM, respectively, with a 1 : 1 stoichiometry between **40** and ATP. Interestingly, in CH_3CN, chemosensor **40** was found to exclusively recognize $H_2PO_4^-$ ions over other anions and formed a significant excimer at 455 nm. The stoichiometry of the **40**-$H_2PO_4^-$ complex was found to be 1 : 1 while the binding constant and detection limit were 7.06 × 10^3 M^{-1} and 1.46 μM, respectively. Chemosensor **40** was also used for intracellular ATP detection through fluorescence imaging.

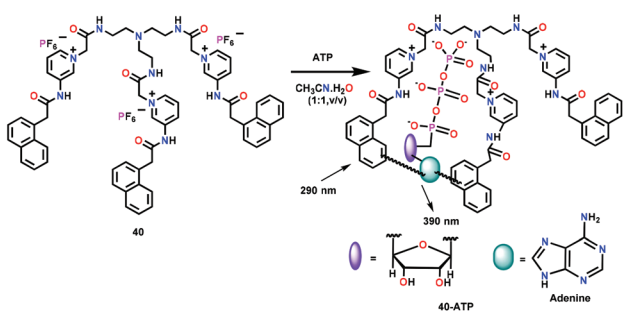

Fig. 18 Chemical drawing of chemosensor **40** and its proposed binding with ATP. Adapted from ref. 63.

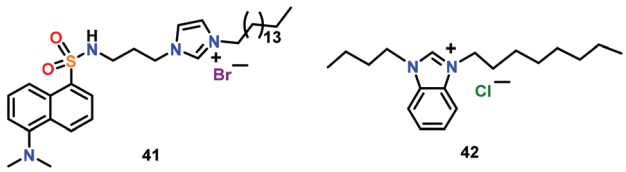

Fig. 19 Chemical drawings of chemosensors **41** and **42**. Adapted from ref. 64 and 65.

Cao and co-workers[64] have reported an amphiphilic receptor **41** for the detection of ATP *via* emission enhancement through anion-induced self-assembly (Fig. 19). Chemosensor **41** was designed by incorporating a dansyl fluorophore. **41** formed self-assembled micelle (CMC = 7.67 μM) in PBS buffer at pH = 7.4. The micelle structure was highly selective for ATP and was found to increase the emission of **41** accompanied by a 27 nm blue shift while exhibiting a green emission at 508 nm. A 1 : 1 stoichiometry, a binding constant of 2.8 × 10^5 M^{-1} and a detection limit of 150 nM were calculated for the detection of ATP. Both the significant change in the fluorescence intensity and blue shift were related to the strong interaction of **41** with ATP through imidazolium C–H and amide NH donors. The binding of ATP decreased the electron withdrawing ability of the sulphonyl group and inhibited internal charge transfer (ICT) occurring through the dimethylamino group to the sulfonyl moiety, thus, causing the fluorescent emission to shift towards a lower wavelength. High selectivity of **41** for ATP was utilized for its sensing in the living cells.

Kang and co-workers[65] have reported a benzimidazolium based ionic liquid **42** for the detection of ADP (Fig. 19). Chemosensor **42** formed micelles in the aqueous medium (pH = 7) and detected ADP over ATP and AMP *via* 'Turn-On' emission. Such an emission enhancement was due to the stabilization of an ADP-micelle ensemble *via* close proximity of the benzimidazolium moiety and ADP. The binding constant and detection limit for ADP were found to be 1.5 × 10^8 M^{-1} and 1.63 nM, respectively.

4. Metal complex based chemosensors

In this section, we have discussed metal complex based chemosensors for the detection of different types of phosphates *via* a luminescent 'Turn-On' mechanism. In general, metal ion(s) in such complexes provided coordination sites for the recognition of the phosphate group(s) whereas the attached ligands were found to participate in other types of interactions.

4.1. Detection of mono-phosphates (PO_4^{3-}, HPO_4^{2-}, and $H_2PO_4^-$)

In this section, we have summarized metal complex based chemosensors used for the 'Turn-On' detection of mono-phos-

phates such as PO_4^{3-}, HPO_4^{2-} and $H_2PO_4^-$. Ghosh and co-workers[66] have developed several luminescent Ru(II)–polypyridyl complexes for the recognition of different phosphates, mainly $H_2PO_4^-$ and $HP_2O_7^{3-}$ ions. Such Ru–polypyridyl complexes functioned as the excellent phosphorescent chemosensors due to their unique optical properties such as long excited-state lifetime, visible region excitation, large Stokes shift and red-orange emission. The mononuclear Ru(II) complex **43** containing pyridine–triazolium and phenanthroline ligands was used for the sensing of $H_2PO_4^-$ ions and to a lesser extent $HP_2O_7^{3-}$ ion (Fig. 20). Chemosensor **43** exhibited ligand-based π···π transitions at 262 nm while the characteristic MLCT bands appeared at 403 nm (Ru-to-phenanthroline) and 445 nm (Ru-to-pyridyl-triazolium). Chemosensor **43** showed a weak emission band at 590 nm on exciting at either λ_{ex} = 403 or 445 nm. The absorption as well as emission spectra of **43** showed significant changes both with the $H_2PO_4^-$ and $HP_2O_7^{3-}$ ions in CH_3CN. The emission intensity of **43** was increased by 6-fold by $H_2PO_4^-$ and 3-fold by the $HP_2O_7^{3-}$ ion, accompanied by a 10 nm red-shift. Upon sequential addition of $H_2PO_4^-$ and $HP_2O_7^{3-}$ ions, absorption spectral features at 403 and 455 nm showed a marginal decrease with an increase at 465 nm. These spectral titrations provided binding constants ($K_b \times 10^4$ M^{-1}) of 5.28 and 4.67 for $H_2PO_4^-$ and $HP_2O_7^{3-}$ ions, respectively, whereas detection limits were 0.25 and 0.45 μM, respectively. The lifetime of chemosensor **43** (5.45 ns) increased to 28.60 and 12.01 ns in the presence of $H_2PO_4^-$ and $HP_2O_7^{3-}$ ions, respectively. These parameters displayed strong affinity of **43** towards $H_2PO_4^-$ as compared to the $HP_2O_7^{3-}$ ion. ^{31}P NMR spectral studies confirmed the participation of phosphate–O groups in bonding while a proton NMR spectrum showed a gradual downfield shift of the triazole proton. Finally, X-ray structural studies confirmed pyrophosphate ion binding *via* C–H···diphosphate interactions (Fig. 20).

Encouraged by the remarkable phosphate selectivity of Ru(II)–polypyridyl complex **43** *via* C–H···anion interactions, Ghosh and co-workers developed[67] a halogen bonding (X-bonding) based anion receptor **44** by substituting the triazole–C–H group with triazole–C–I to enhance the phosphate selectivity (Fig. 21). For comparative studies, an analogous compound **45** was also synthesized. Both Ru(II)–polypyridyl based chemosensors **44** and **45** displayed similar UV-Vis and

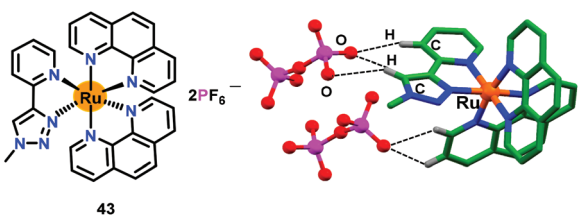

Fig. 20 Chemical drawing of chemosensor **43** and the crystal structure of **43**·$H_2P_2O_7^{2-}$. Hydrogen atoms, except for those involved in H-bonding interactions, have been omitted for clarity. Adapted from ref. 66.

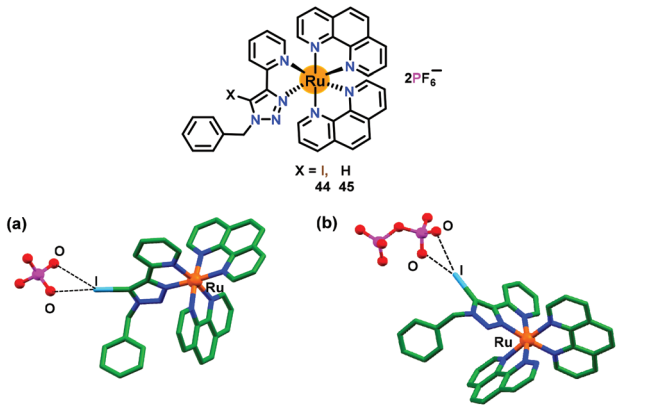

Fig. 21 Chemical drawings of chemosensors **44** and **45**. Crystal structures of (a) **44**·$H_2PO_4^-$ and (b) **45**·$HP_2O_7^{3-}$ complexes. Adapted from ref. 67.

emission spectra and anion binding properties as noted for **43**. Both **44** and **45** detected $H_2PO_4^-$ ions preferably over $HP_2O_7^{3-}$ as compared to other anions in CH_3CN. The emission of **44** increased both with $H_2PO_4^-$ (17-fold) and $HP_2O_7^{3-}$ ions (5-fold) in CH_3CN. The binding constants ($K_b \times 10^4$ M^{-1}) were noted as 19.4 and 5.60 for $H_2PO_4^-$ and $HP_2O_7^{3-}$ ions, respectively, while detection limits were 0.018 μM and 0.090 μM, respectively. Similarly, binding constants ($K_b \times 10^3$ M^{-1}) for the analogous **45** were, respectively, 55.9 and 9.71 for $H_2PO_4^-$ and $HP_2O_7^{3-}$ ions, whereas detection limits were 0.05 μM and 0.25 μM, respectively. Both chemosensors **44** and **45** also worked as the lifetime based detectors where excited-state lifetimes for the free **44** and **45** enhanced both with $H_2PO_4^-$ and $HP_2O_7^{3-}$ ions. Remarkably, chemosensor **44** with an I donor functioned as a superior sensor with higher binding affinities and greater excited-state lifetime enhancement when compared to its H–analogue (**45**). The crystal structure of **44** with $H_2PO_4^-$ and $HP_2O_7^{3-}$ ions confirmed the presence of C–I···anion X-bonding interactions (Fig. 21a and b).

After the successful incorporation of the triazole–C–I group into the Ru(II)–polypyridyl complex, Ghosh and co-workers[68] integrated an additional anion binding urea arm in the triazole unit (Fig. 22). The chemosensor **46** bearing a triazole unit accompanied by an appended 4-fluorophenyl group was used for the sensing of anions. Chemosensor **46** was crystallographically characterized where a ruthenium ion exhibited a distorted octahedral geometry coordinated by two phenanthroline ligands and a pyridine–triazole unit (Fig. 22a). The binding constants ($K_b \times 10^4$ M^{-1}) for **46** were found to be 15.0 and 4.1 for $H_2PO_4^-$ and $HP_2O_7^{3-}$ ions, respectively, while detection limits were 0.36 μM and 0.54 μM, respectively. In a similar manner, excited state lifetime of free **46** was enhanced in the presence of $H_2PO_4^-$ and $HP_2O_7^{3-}$ ions. These parameters showed strong affinity of **46** towards $H_2PO_4^-$ as compared to $HP_2O_7^{3-}$ ions. Notably, chemosensor **46** showed better sensing for phosphates in comparison with the non-urea analogue **43**.

Ghosh and co-workers[69] further developed two related chemosensors, **47** and **48**, having pentafluorophenylurea and

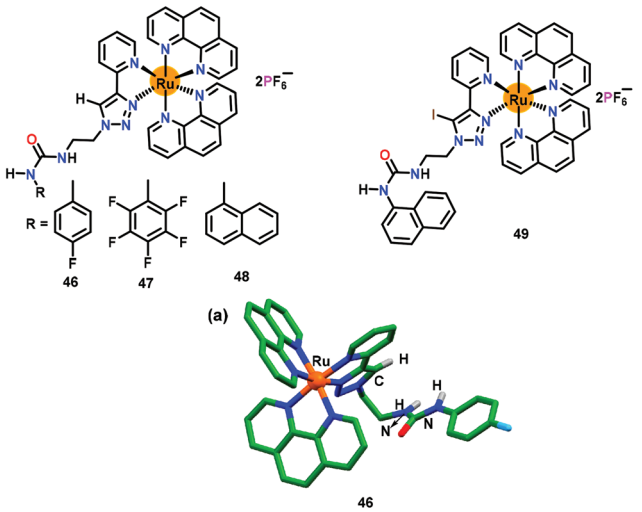

Fig. 22 Chemical drawings of chemosensors **46–49**. (a) Crystal structure of chemosensor **46**; hydrogen atoms, except for the N–H groups, have been omitted for clarity. Adapted from ref. 68–70.

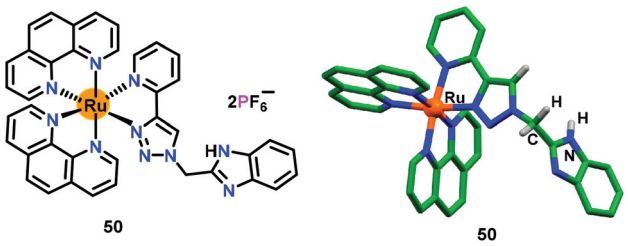

Fig. 23 Chemical drawing and crystal structure of chemosensor **50**. Hydrogen atoms, except for the N–H and CH_2 groups, have been omitted for clarity. Adapted from ref. 71.

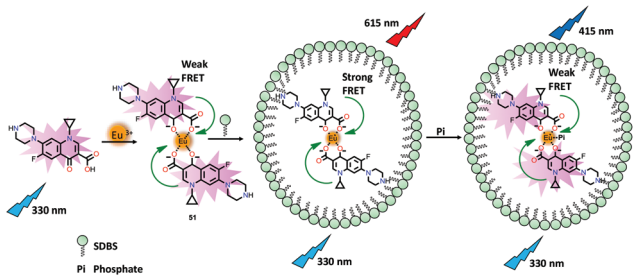

Fig. 24 Chemical drawings of ciprofloxacin and its Eu(III) complex **51** that has been used for the detection of PO_4^{3-} ions based on FRET from ciprofloxacin to Eu(III) ions induced by the surfactant SDBS. Adapted from ref. 72.

1-naphthylurea, respectively (Fig. 22). High binding constants (10^4–10^5 M^{-1}), detection limits (0.020 and 0.580 μM) and excited state lifetimes were noted both for **47** and **48**. Collectively, chemosensor **47** having acidic –NH urea protons revealed higher binding affinities for phosphates when compared to analogous chemosensors **46** and **48** (with urea) and **43** and **45** (non-urea).

Finally, to develop an effective phosphate sensor, Ghosh and co-workers[70] synthesised iodotriazole linked naphthyl urea based receptor **49** (Fig. 22). The binding constants (K_b × 10^5 M^{-1}) for **49** were 12.3 and 8.6 for $H_2PO_4^-$ and $HP_2O_7^{3-}$ ions, respectively, whereas detection limits were 0.012 μM and 0.078 μM, respectively. Chemosensor **49** also showed excited-state lifetime enhancement from 10.7 ns (for free **49**) to 206.1 ns and 101.1 ns for $H_2PO_4^-$ and $HP_2O_7^{3-}$ ions, respectively. Chemosensor **49** was superior for phosphate binding in view of its high binding constant, lower detection limit and longer excited state lifetime as compared to other analogues, **43–48**.

Similar to **43–49**, Khatua and co-workers[71] have developed a benzimidazole appended 1,2,3-triazole-pyridyl based chemosensor **50** which was crystallographically characterized (Fig. 23). Chemosensor **50** was used for the exclusive detection of $H_2PO_4^-$ and $HP_2O_7^{3-}$ ions in CH_3CN. The emission at 583 nm showed 10-fold enhancement after the addition of $HP_2O_7^{3-}$ and $H_2PO_4^-$ ions. The binding constants (K_b × 10^3 M^{-1}) were noted as 6.8 and 3.3 whereas detection limits were 5.19 and 5.73 ppb for $HP_2O_7^{3-}$ and $H_2PO_4^-$ ions, respectively. ^1H NMR spectral studies displayed downfield shifts for the triazole–CH protons which established its interaction with phosphate ions.

Tong and co-workers[72] have reported a Eu(III) based chemosensor **51** for the exclusive detection of PO_4^{3-} ions in aqueous medium (Fig. 24). The detection limit towards the PO_4^{3-} ion was found to be 4.3 nM which made it an excellent chemosensor for environmental water samples. The authors employed a new strategy by using a FRET sensitizer sodium dodecylbenzenesulfonate (SDBS) surfactant[73] for the detection of PO_4^{3-} ions. The intense blue emission for the free ligand at 415 nm (λ_{ex} = 330 nm) was quenched to some extent after the formation of **51** due to FRET from the ligand to the Eu(III) centre. Interestingly, this FRET process was not effective to produce the fingerprint bands of the Eu(III) centre at around 615 nm ($^5D_0$–$^7F_2$). Interestingly, the FRET process was promoted when the carboxylate groups of **51** interacted with SDBS. Consequently, the PO_4^{3-} ion selectively interacted with the Eu(III) center of **51** and significantly reduced the FRET process which enhanced the emission at 415 nm.

4.2. Detection of di-phosphates (pyrophosphate ion (PPi) and its derivatives)

In this section, metal complex based chemosensors have been discussed for the recognition of the pyrophosphate ion (PPi) and its derivative *via* a 'Turn-On' emission mechanism.

Gupta and co-workers[74] have developed several related chemosensors based on phenol-derivatives while additionally containing an alcohol and an imine group for the recognition of Al^{3+} and Ga^{3+} ions. **Pro-52** efficiently detected Al^{3+} and Ga^{3+} ions *via* 'Turn-On' emission in EtOH (containing 0.5% THF). Notably, the resultant Al^{3+} and Ga^{3+} based species **52** and **53** were able to further detect the pyrophosphate ion (PPi) and therefore functioned as the chemosensors (Fig. 25). **Pro-52** showed emission enhancement with Al^{3+} (9-fold) and Ga^{3+}

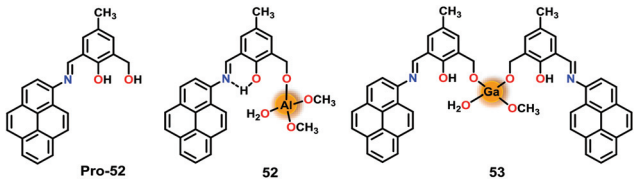

Fig. 25 Chemical drawings of **Pro-52** and chemosensors **52** and **53**. Adapted from ref. 74.

(3.8-fold) ions, suggesting the formation of **52** and **53**. Consequently, addition of PPi further enhanced the emission by 2.5-fold and 4.4-fold for **52** and **53**, respectively. Detailed mechanistic studies illustrated that PPi acted as a base and deprotonated the intact phenolic–OH group in **52** and **53**. In the ^{1}H NMR spectra, **52** and **53** showed a phenolic–OH signal at δ = 13.7 ppm which was noted to disappear in the presence of the $P_2O_7^{4-}$ ion (PPi). The presence of PPi also produced a visible color change from pale pink to dark green. The pyrophosphate ion mediated deprotonation of **52** and **53** was further supported by the DFT studies.

Earlier, Ghosh and co-workers have used Ru(II)–polypyridyl based chemosensors **43–49** for the selective sensing of $H_2PO_4^-$ over $HP_2O_7^{3-}$ ion.[66–70] Subsequently, these authors developed[75] a trinuclear chemosensor **54** for the detection of phosphates (Fig. 26). Chemosensor **54** revealed similar photophysical properties as noted for **43–49**.[66–70] Detailed sensing studies revealed that while chemosensors **43–49** were highly selective towards $H_2PO_4^-$ over $HP_2O_7^{3-}$ ion, **54** exhibited selective detection of $HP_2O_7^{3-}$ over $H_2PO_4^-$ ion. Thus, a reverse selectivity was observed for different phosphates on changing

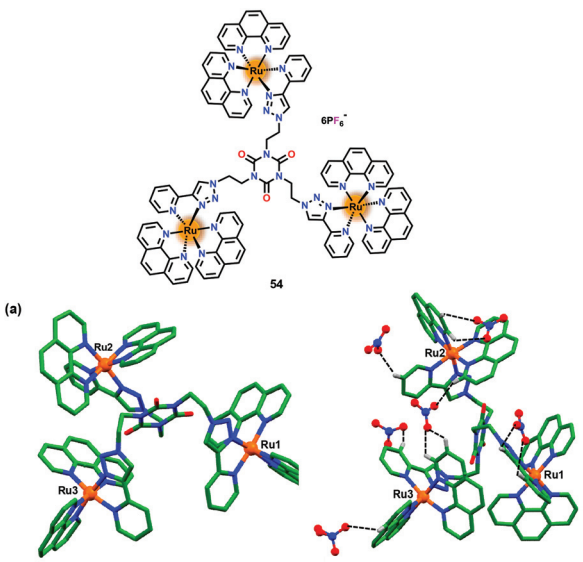

Fig. 26 Chemical drawing of chemosensor **54**. (a) Crystal structure of chemosensor **54** and (b) its nitrate complex displaying various C–H···O interactions between C–H groups and nitrate–O atoms. Hydrogen atoms, except for those involved in weak interactions, have been omitted for clarity. Adapted from ref. 75.

a receptor from mononuclear to trinuclear one. Mononuclear receptors **43–49** possessed a single triazole –C–H unit for anion binding which preferred to bind a single negatively charged and smaller phosphate ion, $H_2PO_4^-$. In contrast, trinuclear yet flexible **54**, containing multiple binding sites, preferred to interact with a more negatively charged and bulkier phosphate ion, $HP_2O_7^{3-}$ ion. Emission spectral studies confirmed the formation of a 1 : 3 H : G complex between **54** and $HP_2O_7^{3-}$/$H_2PO_4^-$ ions. The overall binding constants ($K_b \times 10^{13}$ M^{-3}) were 6.76 and 91.2 whereas detection limits were noted to be 0.02 and 0.45 mM for $HP_2O_7^{3-}$ and $H_2PO_4^-$ ions, respectively. Interestingly, **54** showed enhancement in the excited state lifetime (4.78 ns) in the presence of $H_2PO_4^-$ (8-times) and $HP_2O_7^{3-}$ (28-times). Furthermore, in different media (10% Tris-HCl buffer–90% CH_3CN) **54** showed selectivity for AMP, ADP and ATP over $HP_2O_7^{3-}$ and $H_2PO_4^-$ ions. The presence of multiple C–H···anion interactions was confirmed by the single crystal analysis of only chemosensor **54** (Fig. 26a) and its nitrate-complex (Fig. 26b). Notably, various weak C–H···O interactions were noted between the acidic C–H protons of the triazole unit and the phenanthroline moiety to that of nitrate ions.

Li and co-workers[76] have reported a dinuclear Zn-based chemosensor **55** containing chelating units bridged by a BINOL fluorophore for the detection of $HP_2O_7^{3-}$ ions in HEPES buffer (1% CH_3OH) (Fig. 27). The presence of Zn^{2+} ions induced a 'Turn-On' florescence at 383 nm (λ_{ex} = 316 nm). The addition of $HP_2O_7^{3-}$ ions further enhanced the emission at 383 nm while generating a 1 : 1 complex with **55**. The K_b was noted to be 6.7×10^5 M^{-1} while the detection limit was 95 nM. The 'Turn-On' detection of $HP_2O_7^{3-}$ ions was owing to the overall rigidity of the system and the optimal distance between the two Zn^{2+} ions. Interestingly, chemosensor **55** also showed precipitation-based detection of $HP_2O_7^{3-}$ ions at millimolar concentrations. Chemosensor **55** was successfully used for the detection of $HP_2O_7^{3-}$ ions in the living cells.

Feng and co-workers[77] have reported a phenol-bridged dinuclear Zn(II) complex **56** appended with a dicyanomethylene–benzopyran group exhibiting near-infrared emission at 639 nm (Fig. 27). Chemosensor **56** selectively sensed $HP_2O_7^{3-}$ ions over other anions in HEPES buffer (pH = 7.4). Interestingly, addition of 0.5 equiv. of $HP_2O_7^{3-}$ ions showed an

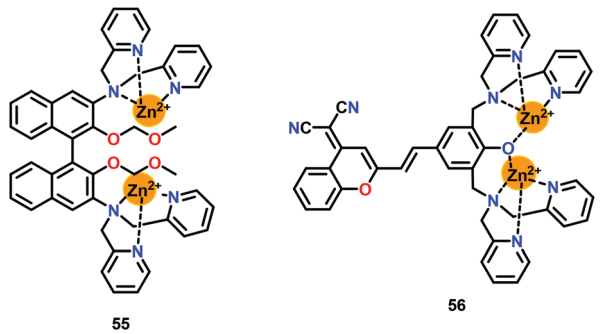

Fig. 27 Chemical drawings of chemosensors **55** and **56**. Adapted from ref. 76 and 77.

initial emission quenching with a 14 nm red-shift. Consequently, further addition of $HP_2O_7^{3-}$ ions exhibited emission enhancement at 654 nm. The initial emission quenching at low concentration of $HP_2O_7^{3-}$ ions was due to the PET process from DPA moieties to the fluorophore. However, a stable **56**-$HP_2O_7^{3-}$ complex was formed at higher concentration of PPi while the ICT process was responsible for the emission enhancement. The detection of $HP_2O_7^{3-}$ ions by **56** was accompanied by a Stokes shift of 150 nm. Chemosensor **56** also showed an excellent colorimetric detection by exhibiting colour change from orange to pink with PPi in aqueous medium. A 1 : 1 **56**-$HP_2O_7^{3-}$ complex was formed between **56** and PPi with a detection limit of 42 nM. Chemosensor **56** was found to operate over a wide pH range (6.05–9.70) and was also used in the cell imaging studies owing to its very low cytotoxicity.

Yam and co-workers[78] have reported a terpyridine-coordinated platinum and DPA-coordinated zinc based chemosensor **57** for the detection of PPi in HEPES buffer (containing 30% CH_3CN; pH 7.4) (Fig. 28). The UV–Vis spectral titration of **57** with PPi shows an increase in the 650 nm band assigned to dσ*(Pt···Pt) → π*(terpy) and a concomitant decrease in 415 nm band accompanied by an isosbestic point at 347 nm. A colour change from yellow to orange was observed for chemosensor **57** with PPi. The emission spectrum of chemosensor **57** with PPi showed an enhancement at 770 nm with a concomitant decrease in the higher-energy band at 600 nm, signifying the formation of aggregates. The formation of oligomers between **57** and PPi was confirmed by the spectroscopic studies. In ^{1}H NMR spectral titration, aromatic-H signals of **57** were up-field shifted due to the aggregate formation. In electron microscopy studies, **57** was found to be randomly dispersed without any aggregation; however, upon addition of 1.5 equiv. of PPi, **57** formed long fibre-like aggregates. The energy dispersive X-ray (EDX) analysis revealed the presence of Pt, Zn and P elements in the aggregates. PPi formed a $(\mathbf{57})_2$**·PPi** adduct with **57** through intermolecular Pt···Pt interactions (3.4 Å) wherein PPi was held between two zinc centres.

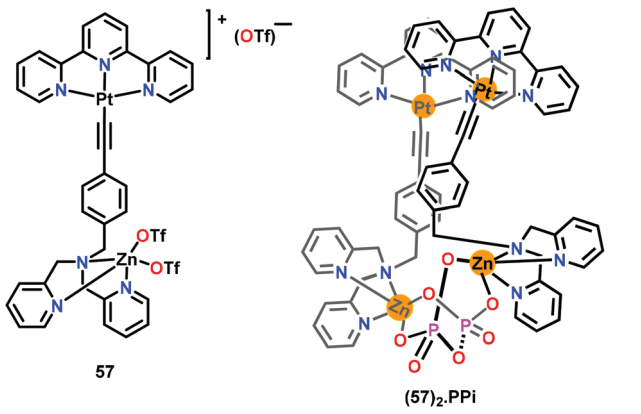

Fig. 28 Chemical drawing of chemosensor **57** and its PPi complex $(\mathbf{57})_2$**·PPi**. Adapted from ref. 78.

4.3. Detection of adenosine phosphates (AMP, ADP and ATP)

In this section, metal complex based chemosensors have been discussed for the detection of adenosine phosphates (AMP, ADP and ATP) *via* the 'Turn-On' emission mechanism.

Gupta and co-workers[79] have reported hydroxide-bridged dizinc(II) complexes, **58–51**, presenting a H-bonding based cavity (Fig. 29). In these complexes, the Zn-bound hydroxide group behaved as an H-bond donor to the heterocyclic rings which functioned as the H-bond acceptors. In contrast, *para*-anisidine appended rings in **61** were deprived of any H-bonding groups and thus the hydroxide group was not involved in any H-bonding. These chemosensors exhibited emission at *ca.* 510 nm (λ_{ex} = 330 nm for **58–60** and 350 nm for **61**) in a DMSO/HEPES buffer (9 : 1, v/v; pH 7.2). Importantly, chemosensors **58** and **59** showed nearly six-fold emission enhancement with ATP whereas negligible changes were observed with other phosphates and other anions. In contrast, **60** and **61** did not exhibit any considerable emission spectral change with any of the phosphates including ATP. The binding stoichiometry between **58** and **59** to that of ATP was found to be 1 : 1 while binding constants ($K_b \times 10^5$ M^{-1}) were 7.5 and 11.1, respectively. The ATP detection limits for **58** and **59** were 59 nM and 10.1 nM, respectively. ^{31}P NMR spectral studies revealed the interaction of ATP with **58** and **59** as the phosphorus nuclei of ATP experienced a downfield shift. The H-bonding based cavity in **58** and **59** played a crucial role in the detection of ATP. In these complexes, synergistic effects involving zinc sites for coordinating the phosphate groups of ATP and H-bonding as well as π···π stacking between pyridine ring of a zinc complex and the adenine ring of ATP were together responsible for the unique sensing of ATP. Complex **61**, which lacked H-bonding functional groups due to the involvement of *para*-anisole groups, did not recognize ATP.

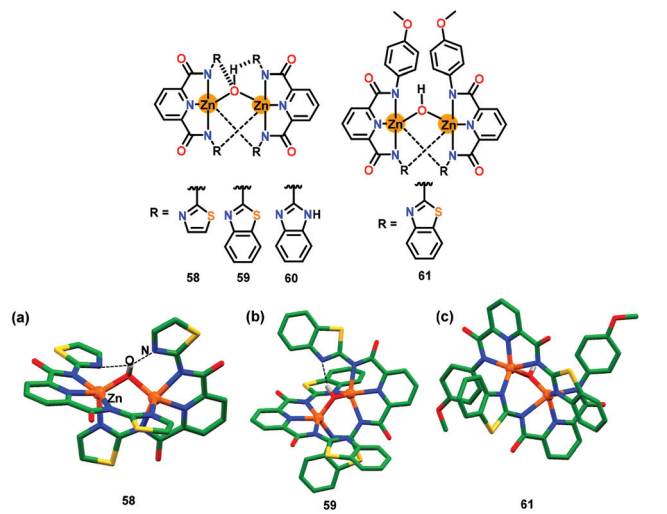

Fig. 29 Chemical drawings of chemosensors **58–61**. Crystal structures of chemosensors (a) **58**, (b) **59** and (c) **61**. Hydrogen atoms, except for the bridged hydroxide group, have been omitted for clarity. Adapted from ref. 79.

Das and co-workers[80] have developed a mononuclear zinc-based chemosensor **62** for the efficient detection of higher phosphates (Fig. 30). The Zn(II) ion was coordinated to a DPA chelate unit while the appended coumarin moiety acted as the fluorescent probe. Chemosensor **62** showed detection of both ADP and ATP *via* 'Turn-On' emission at 500 nm (λ_{ex} = 400 nm) in aqueous medium (HEPES, pH = 7.4) by forming **62**-ATP and **62**-ADP adducts while exhibiting very good detection limits of 8.4 nM (ATP) and 12.5 nM (ADP). ^{31}P NMR spectral studies revealed that both ADP and ATP were found to bind with **62** through their phosphate groups. ^{1}H NMR spectroscopy was used for evaluating interaction of the diphosphate or triphosphate unit of ADP or ATP with the Zn(II) center and for calculating the binding affinities. Chemosensor **62** exhibited a large Stokes shift (*ca.* 100 nm) while its recognition ability allowed evaluating the ATP concentration change within the mitochondria.

Moro and co-workers[81] have developed a zinc-based chemosensor **63** bearing naphthalimide linked DPA unit for the detection of ATP (Fig. 31). The DPA based chelating unit coordinated with the Zn(II) ion while the naphthalimide fluorophore was free for the spectroscopic changes. A 2.3-fold emission enhancement at 535 nm was noted upon the introduction of ATP while saturation was noted at 10 mM concentration. The fluorescent quantum yield was enhanced from 0.28 for free **63** to 0.57 for the **63**-ATP adduct. The interaction of ATP with Zn–DPA unit of chemosensor **63** decreased the strength of the Zn^{2+}–N bonding interactions which resulted in the emission enhancement. Chemosensor **63** also detected other phosphates such as ADP and PPi but only in the micromolar range while a larger change in the emission was noted only with ATP.

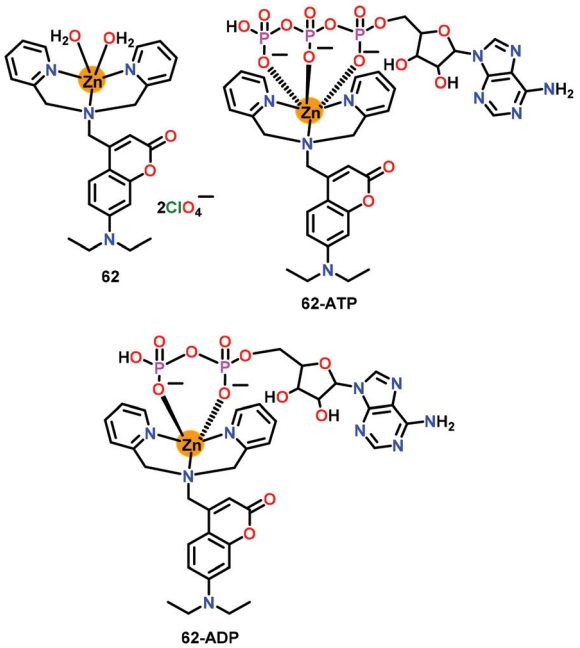

Fig. 30 Chemical drawing of chemosensor **62** and its **62**·ATP and **62**·ADP complexes. Adapted from ref. 80.

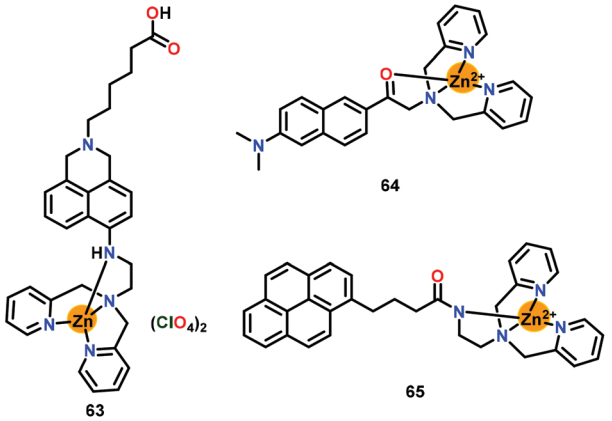

Fig. 31 Chemical drawings of chemosensors **63**–**65**. Adapted from ref. 81–83.

Kim and co-workers[82] have reported a Zn(II)–DPA based chemosensor **64** containing 6-acetyl-2-(dimethylamino) naphthalene (acedan) as a two-photon fluorophore (Fig. 31). This two-photon chemosensor showed significant absorption/emission spectral changes with ATP over other phosphates (ADP, AMP and $HP_2O_7^{3-}$) in HEPES buffer (containing 1%-CH_3CN; pH = 7.4). In the presence of ATP, chemosensor **64** showed an absorption spectral change at 410 nm accompanied by a 10 nm hypsochromic shift. On the other hand, emission spectral titration against 2 equiv. of ATP showed 8.5-fold enhancement. The quantum yield for the **64**-ATP adduct illustrated 5-fold enhancement when compared to free **64**. The binding constants ($K_b \times 10^5$ M^{-1}) from the emission spectral titration were 0.05 (AMP), 3.2 (ADP), 40.0 (PPi) and 62.0 (ATP). The NMR and emission spectral studies suggested the occurrence of π···π interactions between the fluorophore and the nucleobases. The 'Turn-On' detection was due to the coordination of the carbonyl group to the Zn^{2+} center. Chemosensor **64** was also used for the effective detection of ATP and ADP in live cells.

Xing and co-workers[83] have designed a Zn–DPA based chemosensor **65** containing a pyrene fluorophore for the selective detection of ATP and ADP over other phosphates and anions (Fig. 31). Chemosensor **65** showed a significant emission response and change in the proton NMR spectra with both ATP and ADP. Notably, ATP induced excimer emission at 482 nm while also enhancing the monomer emission at 390 nm. However, ADP comparatively resulted in smaller enhancement of the excimer emission but large enhancement of the monomer emission. The binding constants ($K_b \times 10^{10}$ M^{-2}) were calculated as 3.6 and 0.71 for ATP and ADP, respectively. It was found that both **65**-ATP and **65**-ADP adducts have similar stabilities in aqueous medium and formed intramolecular sandwich structures. Authors provided spectroscopic evidence that in **65**-ATP the adenine ring was outside the pyrene dimer of two molecules of **65** while the phosphate part was coordinated to two zinc centers. However, in **65**-ADP, the adenine ring was between pyrene dimers to form a fully intramolecular sandwich structure.

Hamachi and co-workers[84] have developed a dinuclear Zn-based chemosensor **66** containing an anthracene bridge as the fluorophore while having appended DPA groups as the chelating units (Fig. 32). The emission of the anthracene unit at 460 nm (λ_{ex} = 380 nm) showed 3-fold enhancement with ATP over ADP and AMP in HEPES buffer (pH 7.2). A 1 : 1 stoichiometry was noted between **66** and ATP by the emission spectral titration while binding constants ($K_b \times 10^4$ M^{-1}) were noted to be 220 (ATP), 22 (ADP) and 6.6 (AMP). Binding of **66** with ATP was also confirmed by the downfield shifting of β and γ signals of ATP in the ^{31}P NMR spectra, suggesting that **66** binds only with β and γ phosphates and not with α. The quantity of anionic charges on an analytes played an important role whereas the order of selectivity was found to be ATP > ADP > AMP. Thus, poly-anionic ATP showed highest interaction with the cationic Zn(II) centers of **66** rather than ADP and AMP.

Hamachi and co-workers[85] further developed a DPA based dizinc chemosensor **67** containing xanthene as the fluorophore for ATP sensing (Fig. 32). Structurally characterized chemosensor **67** (Fig. 32a) exhibited a weak emission at 522 nm and an absorption spectral band at 509 nm in HEPES buffer (pH 7.4). Chemosensor **67** selectively recognized ATP with a significant emission enhancement, high binding affinity (K_b = 1.3 × 10^6 M^{-1}), 1 : 1 stoichiometry and high quantum yield (φ = 0.61). The 'Turn-On' recognition of ATP was manifested by the formation of a conjugated xanthene form from its non-fluorescent de-conjugated form which was generated by the nucleophilic attack of Zn-bound H_2O.

Chen and co-workers[86] have presented two simple terpyridine based Zn(II) complexes **68** and **69** for the detection of ATP (Fig. 33). The crystal structure of chemosensor **69** was substantiated by X-ray crystallography. Both chemosensors **68** and **69** functioned through two-component metallo–hydrogel formation for the detection of ATP. The weak emission of **68** at 617 nm (λ_{ex} = 448 nm) was enhanced with ATP (44-fold) and ADP (14-fold) while no emission change was found with other anions. The detection limit for ATP was observed as 1.85 μM in aqueous medium. On the other hand, chemosensor **69** displayed a good emission at 450 nm (λ_{ex} = 284 nm) but showed very small changes in its emission at 450 nm with phosphates and other anions; however, a slight quenching was observed with ATP. The linear geometry of **68** assisted it to form a self-assembly with ATP and that enhanced the emission due to AIE. The geometry of the resultant adduct was strongly influenced by the intramolecular π-stacking involving aromatic ring of **68** and planar nuclear bases of ATP. Notably, the self-assembly process established a new sensing method. Chemosensor **68** exhibited low cytotoxicity and was thus used for monitoring ATP in HeLa cells by using confocal fluorescence microscopy.

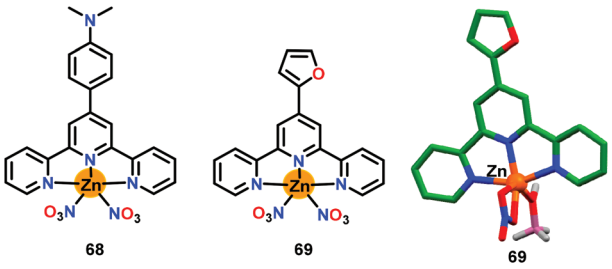

Fig. 33 Chemical drawings of chemosensors **68** and **69** and crystal structure of chemosensor **69**. Adapted from ref. 86.

Tang and co-workers[87] have presented an Eu(III)-based chemosensor **70** for the highly selective recognition of ATP in aqueous medium (Fig. 34). The emission at 615 nm showed enhancement and shifted to 591 nm with ATP. Notably, a 2 : 1 stoichiometry was observed between **70** and ATP with a binding constant of 7.85 × 10^3 M^{-2} and a detection limit of 8.87 μM. The emission enhancement was largely due to the free terpyridine group which enhanced the coordination interaction as well as π···π stacking between ATP and chemosensor **70**.

Subramanian and co-workers[88] have developed an Eu(III)-based chemosensor **71** for the selective recognition of AMP in HEPES buffer (pH = 4) (Fig. 34). The weak emission of **71** was due to the labile water molecules whereas the presence of AMP

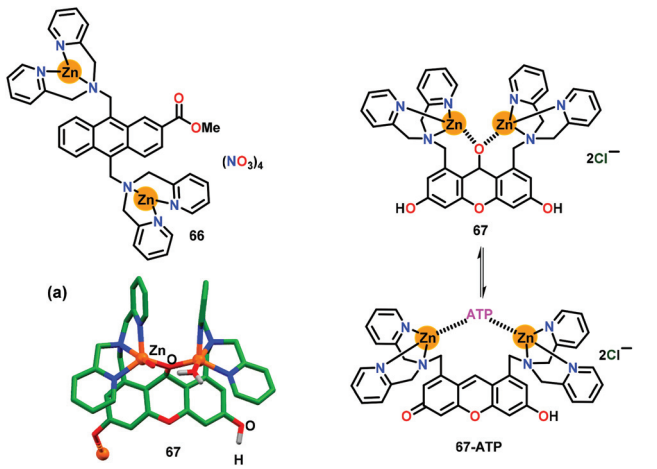

Fig. 32 Chemical drawings of chemosensors **66** and **67**. (a) Crystal structure of chemosensor **67**. Adapted from ref. 84 and 85.

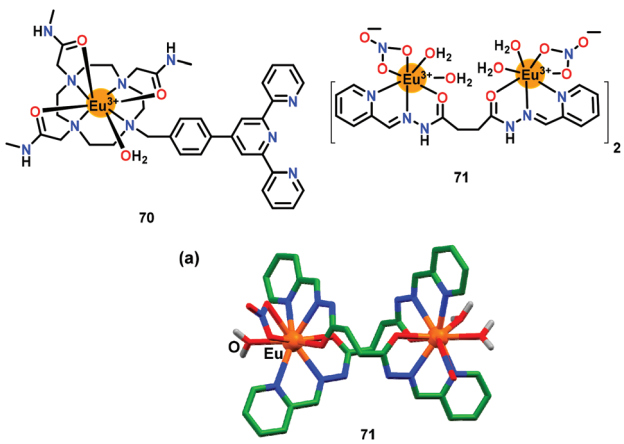

Fig. 34 Chemical drawings of chemosensors **70** and **71**. (a) Crystal structure of chemosensor **71**. Adapted from ref. 87 and 88.

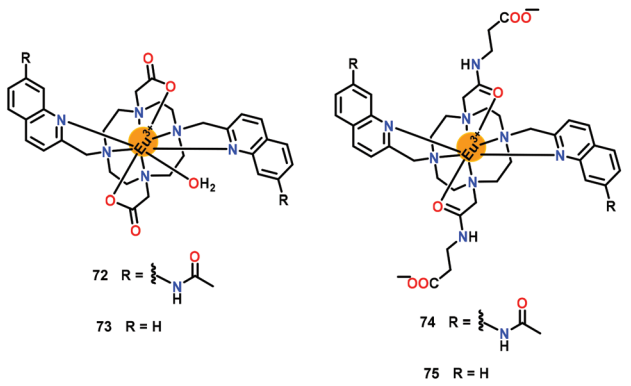

Fig. 35 Chemical drawings of chemosensors **72–75**. Adapted from ref. 89.

led to a 64-fold enhancement in its emission band at 614 nm for the Eu(III) center (λ_{ex} = 320 nm). Chemosensor **71** formed a 1 : 1 stoichiometric adduct with AMP with a K_b value of 6.46 × 10^3 M^{-1} and 2 mM detection limit. The crystal structure showed helical arrangement of both ligands and co-ligands around the Eu(III) ions (Fig. 34a) which were found to be easily replaced by the anions. It was noted that AMP bonded both with the Eu(III) centers by replacing the coordinated H_2O molecules and co-ligands.

Butler and co-workers[89] have presented a series of Eu(III) based chemosensors **72–75** offering different interacting sites (Fig. 35). These chemosensors exhibited significant detection of adenosine phosphates. The absorption spectra of **72** and **74** were very similar and showed a band at 332 nm and 330 nm, respectively. Similarly, both **73** and **75** exhibited absorption maxima at 303 nm and 318 nm, respectively. The emission spectra of **72**, **73** and **75** displayed several similarities with respect to ΔJ = 1 (585–605 nm) the ΔJ = 2 (605–630 nm) bands. Chemosensors **72** and **74** showed excellent selectivity between ATP, ADP and other phosphates due to the presence of carboxamide groups in the pendant arms. Addition of ATP to **72** or **74** resulted in a 10-fold emission enhancement of the ΔJ = 2 band (605–630 nm) while addition of ADP produced a 14-fold emission enhancement. Chemosensors **73** and **75**, which lacked quinoline–amide groups, only manifested 3-fold emission enhancement (ΔJ = 2) with ATP, ADP and AMP. The quinoline groups of **74** sensitized the Eu(III) center whereas terminal phosphate groups of ADP/ATP coordinated to the Eu(III) centers by replacing the labile H_2O molecules. In addition, adjacent phosphate group(s) of ADP/ATP also interacted with the quinoline rings through the H-bonding interactions. Chemosensor **74** formed a 1 : 1 complex both with ATP and ADP with K_b values (×10^5 M^{-1}) of 6.31 and 5.01, respectively.

5. Conclusions and future prospects

The present review article has illustrated several luminescent chemosensors that have been developed for the selective detection of different phosphates through the 'Turn-On' emission response. Such chemosensors were summarized in two broad categories; organic molecule based and metal complex based chemosensors whereas their binding affinities were supplemented with the binding constants and detection limits along with the lifetime parameters. Crystal structures of several free chemosensors as well as their adducts and/or complexes with the assorted anions including phosphates provided structural insights about the mode of interactions between a chemosensor and a guest.

These examples have highlighted several notable take-home design strategies. In the case of organic molecule based chemosensors, the presence of a suitable fluorophore was an essential requirement. In these chemosensors, such fluorophores were largely responsible for the emission output when excited at an appropriate wavelength. The common sensing mechanisms that were mostly prevalent for the detection-led luminescent output were: (i) acid–base strategy where a phosphate ion acted as a base and removed an acidic proton from a chemosensor thus enhancing the conjugation and therefore emission output; (ii) dissociation strategy where a fluorophore was detached from a chemosensor mostly by a hydrolytic pathway; (iii) displacement strategy where a fluorophore was removed from a [chemosensor–fluorophore] adduct; and (iv) interaction strategy where an analyte was noted to interact with a chemosensor *via* various weak interactive forces including H-bonding, anion···π and π···π stacking. On the other hand, the presence of a chelating and/or an interacting site was an essential parameter for the metal complex based chemosensors. In such chemosensors, a phosphate ion was often found to interact with such sites. At the same time, several other non-covalent interactions were clearly observable and cannot be neglected. Several such examples nicely illustrated the significant roles played by the H-bonding, X-bonding, anion···π interaction and π···π stacking as well as other non-conventional weaker interactions.

The examples contained in the present review article have adequately demonstrated that the challenging analytes such as phosphates and adenosine–phosphates that considerably suffer from pH sensitivity and solution dynamics can be conveniently detected both by using organic molecule based and metal complex based chemosensors. At the same time, involvement of phosphates and various adenosine–phosphates in numerous biological processes certainly pose many more challenges in front of the scientific community, particularly in view of live cell imaging and tracking of adenosine–phosphates as well as phosphate-based drugs.[90]

From the environmental perspective, the heavy use of phosphates in detergents, fertilizers, pharmaceuticals, medicines, house-hold products and construction materials is known to contaminate both soil and water bodies.[16–22] Therefore, design of effective chemosensors for phosphates and particularly those that can remove them from the aqueous media while overcoming pH and solvation energy challenges will be timely and pertinent. In this context, intricately designed materials including gels, metal–organic frameworks, zeolites, modified silica and alumina as well as composite materials offer bright prospects.[91–95] Such materials are likely to withstand pH and

solvation energy issues prevailing in the aqueous media and the environmental samples. In the quest for next-generation chemosensor-cum-retrievers, it is desirable to integrate the successful design aspects of molecular chemosensors into robust and reusable materials for not only detection of phosphates but also for their effective removal for much-needed biological and environmental remediation applications. Thus, both the biological and the environmental challenges together with the literature precedents and intelligent design strategies are likely to provide fertile ground and create enormous opportunities for the development of next-generation chemosensors.

Abbreviations

AIE	Aggregation induced emission
ADP	Adenosine diphosphate
AMP	Adenosine monophosphate
ATP	Adenosine triphosphate
BINOL	1,1′-Bi-2-naphthol
CMC	Critical micelle concentration
DFT	Density functional theory
DLS	Dynamic light scattering
DMF	Dimethyl formamide
DMSO	Dimethyl sulphoxide
DPA	2,2′-Dipicolylamine
EDIE	Excimer disaggregation induced emission
EDX	Energy dispersive X-ray spectroscopy
FRET	Free resonance energy transfer
H-bond	Hydrogen bond
H-bonding	Hydrogen bonding
HEPES	(4-(2-Hydroxyethyl)-1piperazineethanesulfonic acid)
ICT	Internal charge transfer
ITC	Isothermal titration calorimetry
IDA	Indicator displacement assay
PBS	Phosphate-buffered saline
PET	Photoinduced electron transfer
PPi	Pyrophosphate
SDBS	Sodium dodecylbenzenesulfonate
SEM	Scanning electron microscopy
TDFT	Time-dependent density functional theory
TEM	Transmission electron microscopy
THF	Tetrahydrofuran
TPE	Tetraphenylethene
TRIS	Trisaminomethane

Conflicts of interest

There are no conflicts to declare.

Acknowledgements

RG gratefully acknowledges financial support from the Science and Engineering Research Board (EMR/2016/ 000888), New Delhi and the Council of Scientific and Industrial Research (01 (2841)/16/EMR-II), New Delhi. PK thanks CSIR, New Delhi for the Senior Research Associateship "Scientists' Pool Scheme" (IA-27577). SP thanks UGC, New Delhi for the SRF fellowship. Reviewers' comments were very helpful during the revision.

References

1 A. V. Gourine, E. Llaudet, N. Dale and K. M. Spyer, ATP is a mediator of chemosensory transduction in the central nervous system, *Nature*, 2005, **436**, 108–111.
2 F. Westheimer, Why nature chose phosphates, *Science*, 1987, **235**, 1173–1178.
3 J. K. Heinonen, *Biological Role of Inorganic Pyrophosphate*, Kluwer Academic Publishers, Norwell, 2001.
4 K. G. Clarke, *Bioprocess Engineering: An Introductory Engineering and Life Science Approach*, Woodhead Publisher, 2013.
5 R. L. P. Adams, J. T. Knowler and D. P. Leader, *The Biochemistry of the Nucleic Acids*, Chapman and Hall, 10th edn, 1986.
6 W. Saenger, *Principles of Nucleic Acid Structure*, Springer-Verlag, 1984.
7 T. S. Moore Jr., Phospholipid biosynthesis, *Annu. Rev. Plant Physiol.*, 1982, **33**, 235–259.
8 J. L. Meiera and M. D. Burkart, The chemical biology of modular biosynthetic enzymes, *Chem. Soc. Rev.*, 2009, **38**, 2012–2045.
9 A. Shaikh, T. Berndt and R. Kumar, Regulation of phosphate homeostasis by the phosphatonins and other novel mediators, *Pediatr. Nephrol.*, 2008, **23**, 1203–1210.
10 J. Gattineni and M. Baum, Genetic disorders of phosphate regulation, *Pediatr. Nephrol.*, 2012, **27**, 1477–1487.
11 C. P. Mathews and K. E. van Hold, *Biochemistry*, The Benjamin/Cummings Publishing Co., Inc., Redwood City, CA, 1990.
12 T. Soderberg, *Organic Chemistry with a Biological Emphasis*, Chemistry Libre Texts Publisher, 2021.
13 W. G. Junger, Immune cell regulation by autocrine purinergic signalling, *Nat. Rev. Immunol.*, 2011, **11**, 201–212.
14 X. Su, C. Zhang, X. Xiao, A. Xu, Z. Xu and M. Zhao, A kinetic method for expeditious detection of pyrophosphate anions at nanomolar concentrations based on a nucleic acid fluorescent sensor, *Chem. Commun.*, 2013, **49**, 798–800.
15 L. Stryer, *Biochemistry*, W. H. Freeman and Company, New York, 4th edn, 1998.
16 C. Rey, in *Calcium phosphates in biological and industrial systems*, ed. Z. Amjad, Kluwer Academic Publishers, Boston, Dordrecht, London, 1998, pp. 217–251.
17 P. A. Gilbert and A. L. Dejong, The use of phosphate in detergents and possible replacements for phosphate, *Ciba Found. Symp.*, 1977, **57**, 253–268.
18 A. N. Sharpley and S. Rekolainen, Phosphorus in agriculture and its environmental implications, in *Phosphorus*

Loss from Soil to Water, ed. H. Tunney, O. T. Carton, P. C. Brookers and A. E. Johnston, CAB International Press, Cambridge, England, 1997, pp. 1–54.

19 F. Nantaba, W.-U. Palm, J. Wasswa, H. Bouwman, H. Kylin and K. Kummerer, Temporal dynamics and ecotoxicological risk assessment of personal care products, phthalate ester plasticizers, and organophosphorus flame retardants in water from Lake Victoria, Uganda, *Chemosphere*, 2021, **262**, 127716–127727.

20 A. M. Rashad, Phosphogypsum as a construction material, *J. Cleaner Prod.*, 2017, **166**, 732–743.

21 K. Chandrasekaran, S. N. T. S. Nellaiappan, R. Kulandaivelu and M. H. Lee, Improving the Reactivity and Receptivity of Alloy and Tool Steels for Phosphate Conversion Coatings: Role of Surface Mechanical Attrition Treatment, *Ind. Eng. Chem. Res.*, 2014, **53**, 20124–20138.

22 C. F. Mason, *Biology of Fresh water Pollution*, Longman, New York, 1991.

23 WHO, *Guidelines for drinking water quantity*, World Health Organization, Geneva, 2nd edn, 1993.

24 E. A. Katayev, Y. A. Ustynyuk and J. L. Sessler, Receptors for tetrahedral oxyanions, *Coord. Chem. Rev.*, 2006, **250**, 3004–3037.

25 H. Chen, L. Zhao, F. Yu and Q. Du, Detection of phosphorus species in water: technology and strategies, *Analyst*, 2019, **144**, 7130–7148.

26 S. Pal, T. K. Ghosh, R. Ghosh, S. Mondal and P. Ghosh, Recent advances in recognition, sensing and extraction of phosphates: 2015 onwards, *Coord. Chem. Rev.*, 2020, **405**, 213128–213184.

27 P. J. Antony, S. Karthikeyan and C. S. P. Iyer, Ion chromatographic separation and determination of phosphate and arsenate in water and hair, *J. Chromatogr. B: Anal. Technol. Biomed. Life Sci.*, 2002, **767**, 363–368.

28 W. Q. Liu, Z. F. Du, Y. Qian and F. A. Li, specific colorimetric probe for phosphate detection based on anti-aggregation of gold nanoparticles, *Sens. Actuators, B*, 2013, **176**, 927–931.

29 E. V. Beletskiy and S. R. Kass, Selective binding and extraction of aqueous dihydrogen phosphate solutions via three-armed thiourea receptors, *Org. Biomol. Chem.*, 2015, **13**, 9844–9849.

30 W. L. Cheng, J. W. Sue, W. C. Chen, J. L. Chang and J. M. Zen, Activated nickel platform for electrochemical sensing of phosphate, *Anal. Chem.*, 2010, **82**, 1157–1161.

31 C. J. Quintana, L. Idrissi, G. Palleschi, P. Albertano, A. Amine, M. El Rhazi and D. Moscone, Investigation of amperometric detection of phosphate: Application in seawater and cyanobacterial biofilm samples, *Talanta*, 2004, **63**, 567–574.

32 D. Talarico, S. Cinti, F. Arduini, A. Amine, D. Moscone and G. Palleschi, Phosphate detection through a cost-effective carbon black nanoparticle-modified screen-printed electrode embedded in a continuous flow system, *Environ. Sci. Technol.*, 2015, **49**, 7934–7939.

33 J. M. Zhu, Y. Shi, X. Q. Zhu, Y. Yang, F. H. Jiang, C. J. Sun, W. H. Zhao and X. T. Han, Optofluidic marine phosphate detection with enhanced absorption using a Fabry-Perot resonator, *Lab Chip*, 2017, **17**, 4025–4030.

34 G. Ji, X. Gao, T. Zheng, W. Guan, H. Liu and Z. Liu, Postsynthetic Metalation Metal–Organic Framework as a Fluorescent Probe for the Ultrasensitive and Reversible Detection of PO_4^{3-} Ions, *Inorg. Chem.*, 2018, **57**, 10525–10532.

35 N. K. Beyeh, I. Diez, S. M. Taimoory, D. Meister, A. I. Feig, J. F. Trant, R. H. S. Ras and K. Rissanen, High-affinity and selective detection of pyrophosphate in water by a resorcinarene salt receptor, *Chem. Sci.*, 2018, **9**, 1358–1367.

36 D. A. McNaughton, M. Fares, G. Picci, P. A. Gale and C. Caltagirone, Advances in fluorescent and colorimetric sensors for anionic species, *Coord. Chem. Rev.*, 2021, **427**, 213573–213616.

37 S. Lee, K. K. Y. Yuen, K. A. Jolliffe and J. Yoon, Fluorescent and colorimetric chemosensors for pyrophosphate, *Chem. Soc. Rev.*, 2015, **44**, 1749–1762.

38 T. Nagano, Development of fluorescent probes for bioimaging applications, *Proc. Jpn. Acad., Ser. B*, 2010, **86**, 837–847.

39 D. H. Joo, J. S. Mok, G. H. Bae, S. E. Oh, J. H. Kang and C. Kim, Colorimetric Detection of Cu^{2+} and Fluorescent Detection of PO_4^{3-} and S^{2-} by a Multifunctional Chemosensor, *Ind. Eng. Chem. Res.*, 2017, **56**, 8399–8407.

40 Y.-X. Yuan, J.-H. Wang and Y.-S. Zheng, Selective Fluorescence Turn-On Sensing of Phosphate Anion in Water by Tetraphenylethylene Dimethylformamidine, *Chem. – Asian J.*, 2019, **14**, 760–764.

41 M. Gao and B. Z. Tang, Fluorescent Sensors Based on Aggregation-Induced Emission: Recent Advances and Perspectives, *ACS Sens.*, 2017, **2**, 1382–1399.

42 J. Zhao, D. Yang, Y. Zhao, L. Cao, Z. Zhang, X.-J. Yang and B. Wu, Phosphate-induced fluorescence of a tetraphenylethene-substituted tripodal tris(urea) receptor, *Dalton Trans.*, 2016, **45**, 7360–7365.

43 J. F. Zhang, L. E. Guo, T. N. Zang, Y. L. Duan, X. Y. Liu, Z. Yang, P. Verwilst, K. Luo, G. K. Wang, J. F. Kou, Y. Zhou and J. S. Kim, Highly Selective In Vivo Imaging of Endogenous/Exogenous Phosphate Ion over ATP and PPi, *Chem. – Asian J.*, 2015, **10**, 1165–1169.

44 L. E. Guo, J. F. Zhang, X. Y. Liu, L. M. Zhang, H. L. Zhang, J. H. Chen, X. G. Xie, Y. Zhou, K. Luo and J. Yoon, Phosphate Ion Targeted Colorimetric and Fluorescent Probe and Its Use to Monitor Endogenous Phosphate Ion in a Hemichannel-Closed Cell, *Anal. Chem.*, 2015, **87**, 1196–1201.

45 A. Kovalchuk, J. L. Bricks, G. Reck, K. Rurack, B. Schulz, A. Szumnac and H. Weißhoffd, A charge transfer-type fluorescent molecular sensor that "lights up" in the visible upon hydrogen bond-assisted complexation of anions, *Chem. Commun.*, 2004, 1946–1947.

46 K. Ghosh, A. R. Sarkar, A. Ghorai and U. Ghosh, Design and synthesis of anthracene-based bispyridinium amides:

anion binding, cell staining and DNA interaction studies, *New J. Chem.*, 2012, **36**, 1231–1245.

47 L. Gonzlez, F. Zapata, A. Caballero, P. Molina, C. R. de Arellano, I. Alkorta and J. Elguero, *Chem. – Eur. J.*, 2016, **22**, 7533–7544.

48 P. Sabater, F. Zapata, A. Caballero, N. de la Visitacion, I. Alkorta, J. Elguero and P. Molina, Comparative Study of Charge-Assisted Hydrogen- and Halogen-Bonding Capabilities in Solution of Two-Armed Imidazolium Receptors toward Oxoanions, *J. Org. Chem.*, 2016, **81**, 7448–7458.

49 F. Zapata, S. J. Benitez-Benitez, P. Sabater, A. Caballero and P. Molina, Modulation of the Selectivity in Anions Recognition Processes by Combining Hydrogen- and Halogen-Bonding Interactions, *Molecules*, 2017, **22**, 2273–2284.

50 J. Yang, C.-C. Dong, X.-L. Chen, X. Sun, J.-Y. Wei, J.-F. Xiang, J. L. Sessler and H.-Y. Gong, Excimer Disaggregation Enhanced Emission: A Fluorescence "Turn-On" Approach to Oxoanion Recognition, *J. Am. Chem. Soc.*, 2019, **141**, 4597–4612.

51 G. Bettistelli, A. Cantelli, G. Guidetti, J. Manzi and M. Monatalti, Ultra–bright and stimuli–responsive fluorescent nanoparticles for bioimaging, *Wiley Interdiscip. Rev.: Nanomed. Nanobiotechnol.*, 2016, **8**, 139–150.

52 P. Sokkalingam, D. S. Kim, H. Hwang, J. L. Sessler and C.-H. Lee, A dicationic calix[4]pyrrole derivative and its use for the selective recognition and displacement-based sensing of pyrophosphate, *Chem. Sci.*, 2012, **3**, 1819–1824.

53 A. C. Sedgwick, J. T. Brewster, T. Wu, X. Feng, S. D. Bull, X. Qian, J. L. Sessler, T. D. James, E. V. Anslyn and X. Sun, Indicator displacement assays (IDAs): the past, present and future, *Chem. Soc. Rev.*, 2021, **50**, 9–38.

54 F. Zapata, A. Caballero, P. Molina, I. Alkorta and J. Elguero, Open Bis(triazolium) Structural Motifs as a Benchmark To Study Combined Hydrogen- and Halogen-Bonding Interactions in Oxoanion Recognition Processes, *J. Org. Chem.*, 2014, **79**, 6959–6969.

55 K. Ghosh, D. Kar, D. Sahub and B. Ganguly, Benzimidazolium-based chemosensors: selective recognition of H_2PO^{4-}, $HP_2O_7^{3-}$, F^- and ATP through fluorescence and gelation studies, *RSC Adv.*, 2015, **5**, 46608–46616.

56 K. Ghosh, A. R. Sarkar, A. Samadder and A. R. Khuda-Bukhsh, Pyridinium-Based Fluororeceptors As Practical Chemosensors for Hydrogen Pyrophosphate ($HP_2O_{7(}^{3-}$) in Semiaqueous and Aqueous Environments, *Org. Lett.*, 2012, **14**, 4314–4317.

57 K.-Y. Tan, C. Li, Y. Li, J. Fei, B. Yang, Y.-J. Fu and F. Li, Real-Time Monitoring ATP in Mitochondrion of Living Cells: a Specific Fluorescent Probe for ATP by Dual Recognition Sites, *Anal. Chem.*, 2017, **89**, 1749–1756.

58 Y. Fang, W. Shi, Y. Hu, X. Li and H. Ma, A dual-function fluorescent probe for monitoring the degrees of hypoxia in living cells via the imaging of nitroreductase and adenosine triphosphate, *Chem. Commun.*, 2018, **54**, 5454–5457.

59 T.-B. Ren, S.-Y. Wen, L. Wang, P. Lu, B. Xiong, L. Yuan and X.-B. Zhang, Engineering a Reversible Fluorescent Probe for Real-Time Live-Cell Imaging and Quantification of Mitochondrial ATP, *Anal. Chem.*, 2020, **92**, 4681–4688.

60 S. Farshbaf and P. Anzenbacher Jr., Fluorimetric sensing of ATP in water by an imidazolium hydrazone based sensor, *Chem. Commun.*, 2019, **55**, 1770–1773.

61 H. Tao, L. He, G. Cheng and Q.-Y. Cao, Linear tetraphenylethene-appended bis-imidazolium salts for sensing of ATP, *Dyes Pigm.*, 2019, **166**, 233–238.

62 H. Ma, M. Yang, C. Zhang, Y. Ma, Y. Qin, Z. Lei, L. Chang, L. Lei, T. Wang and Y. Yang, Aggregation-induced emission (AIE)-active fluorescent probes with multiple binding sites toward ATP sensing and live cell imaging, *J. Mater. Chem. B*, 2017, **5**, 8525–8531.

63 K. Ghosh, D. Tarafdar, A. Samadder and A. R. Khuda-Bukhsh, Pyridinum-based flexible tripodal cleft: a case of fluorescence sensing of ATP and dihydrogenphosphate under different conditions and cell imaging, *RSC Adv.*, 2015, **5**, 35175–35180.

64 J.-H. Zhu, C. Yu, Y. Chen, J. Shin, Q.-Y. Cao and J. S. Kim, A self-assembled amphiphilic imidazolium-based ATP probe, *Chem. Commun.*, 2017, **53**, 4342–4345.

65 G. Singh, M. Kaur, B. A. Shiekh and T. S. Kang, Luminescent micellar nano-interfaces of surface active ionic liquid for the selective recognition of ADP in aqueous medium, *Chem. Commun.*, 2018, **54**, 7463–7466.

66 B. Chowdhury, S. Khatua, R. Dutta, S. Chakraborty and P. Ghosh, Bis-Heteroleptic Ruthenium(II) Complex of a Triazole Ligand as a Selective Probe for Phosphates, *Inorg. Chem.*, 2014, **53**, 8061–8070.

67 B. Chowdhury, S. Sinha and P. Ghosh, Selective Sensing of Phosphates by a New Bis-heteroleptic RuII Complex through Halogen Bonding: A Superior Sensor over Its Hydrogen-Bonding Analogue, *Chem. – Eur. J.*, 2016, **22**, 1–10.

68 T. K. Ghosh, S. Chakraborty, B. Chowdhury and P. Ghosh, Bis-Heteroleptic Ruthenium(II) Complex of Pendant Urea Functionalized Pyridyl Triazole and Phenathroline for Recognition, Sensing, and Extraction of Oxyanions, *Inorg. Chem.*, 2017, **56**, 5371–5382.

69 T. K. Ghosh and P. Ghosh, Balancing the acidity of the pendant urea arm of bis-heteroleptic ruthenium(II) complex containing pyridyl triazole for improved oxyanion Recognition, *Dalton Trans.*, 2018, **47**, 7561–7570.

70 T. K. Ghosh, S. Mondal, S. Bej, M. Nandi and P. Ghosh, An integrated urea and halogen bond donor based receptor for superior and selective sensing of phosphates, *Dalton Trans.*, 2019, **48**, 4538–4546.

71 S. K. Sheet, B. Sen, R. Thounaojam, K. Aguan and S. Khatua, Ruthenium(II) Complex-Based Luminescent Bifunctional Probe for Ag^+ and Phosphate Ions: Ag^+-Assisted Detection and Imaging of rRNA, *Inorg. Chem.*, 2017, **56**, 1249–1263.

72 H. Wu and C. Tong, A Specific Turn-On Fluorescent Sensing for Ultrasensitive and Selective Detection of

Phosphate in Environmental Samples Based on Antenna Effect-Improved FRET by Surfactant, *ACS Sens.*, 2018, **3**, 1539–1545.

73 S. Sandhu, R. Kumar, N. Tripathi, H. Singh, P. Singh and S. Kumar, Lab-on-a-Molecule elaboration for fluorescence based discrimination of commercial surfactants sodium dodecyl sulfate and sodium dodecylbenzenesulfonate, *Sens. Actuators, B*, 2017, **241**, 8–18.

74 V. Kumar, P. Kumar, S. Kumar, D. Singhal and R. Gupta, Turn-On Fluorescent Sensors for the Selective Detection of Al^{3+} (and Ga^{3+}) and PPi Ions, *Inorg. Chem.*, 2019, **58**, 10364–10376.

75 B. Chowdhury, R. Dutta, S. Khatua and P. Ghosh, A Cyanuric Acid Platform Based Tripodal Bis-heteroleptic Ru (II) Complex of Click Generated Ligand for Selective Sensing of Phosphates via C–H···Anion Interaction, *Inorg. Chem.*, 2016, **55**(1), 259–271.

76 S.-Y. Jiao, K. Li, X. Wang, Z. Huang, L. Pu and X.-Q. Yu, Make PyrophosphateVisible: The First Precipitable and Real-time Fluorescent Sensor for Pyrophosphate in Aqueous Solution, *Analyst*, 2015, **140**, 174–181.

77 S. Yang, W. Feng and G. Feng, Development of a near-infrared fluorescent sensor with a large Stokes shift for sensing pyrophosphate in living cells and animals, *Anal. Chim. Acta*, 2018, **1034**, 119–127.

78 Y.-S. Wong, M. Ng, M. C.-L. Yeung and V. W.-W. Yam, Platinum(II)-Based Host–Guest Coordination-Driven Supramolecular Co-Assembly Assisted by Pt···Pt and π–π Stacking Interactions: A Dual-Selective Luminescence Sensor for Cations and Anions, *J. Am. Chem. Soc.*, 2021, **143**, 973–982.

79 D. Bansal and R. Gupta, Selective sensing of ATP by hydroxide-bridged dizinc(II) complexes offering a hydrogen bonding cavity, *Dalton Trans.*, 2019, **48**, 14737–14747.

80 H. Singh, S. Sreedharan, R. Tiwari, C. Walther, C. Smythe, S. K. Pramanik, J. A. Thomas and A. Das, A Fluorescent Chemodosimeter for Organelle-Specific Imaging of Nucleoside Polyphosphate Dynamics in Living Cells, *Cryst. Growth Des.*, 2018, **18**, 7199–7206.

81 A. J. Moro, P. J. Cywinski, S. Korstena and G. J. Mohr, An ATP fluorescent chemosensor based on a Zn(II)-complexed dipicolylamine receptor coupled with a naphthalimide chromophore, *Chem. Commun.*, 2010, **46**, 1085–1087.

82 A. S. Rao, D. Kim, H. Nam, H. Jo, K. H. Kim, C. Ban and K. H. Ahn, A turn-on two-photon fluorescent probe for ATP and ADP, *Chem. Commun.*, 2012, **48**, 3206–3208.

83 Q.-C. Xu, H.-J. Lv, Z.-Q. Lv, M. Liu, Y.-J. Li, X.-F. Wang, Y. Zhang and G.-W. Xing, A pyrene-functionalized Zinc(II)–BPEA complex: sensing and discrimination of ATP, ADP and AMP, *RSC Adv.*, 2014, **4**, 47788–47792.

84 A. Ojida, S.-K. Park, Y. Mito-Oka and I. Hamachi, Efficient fluorescent ATP-sensing based on coordination chemistry under aqueous neutral conditions, *Tetrahedron Lett.*, 2002, **43**, 6193–6195.

85 A. Ojida, I. Takashima, T. Kohira, H. Nonaka and I. Hamachi, Turn-On Fluorescence Sensing of Nucleoside Polyphosphates Using a Xanthene-Based Zn(II) Complex Chemosensor, *J. Am. Chem. Soc.*, 2008, **130**, 12095–12101.

86 W. Fang, C. Liu, F. Yu, Y. Liu, Z. Li, L. Chen, X. Bao and T. Tu, Macroscopic and Fluorescent Discrimination of Adenosine Triphosphate via Selective Metallo-hydrogel Formation: A Visual, Practical, and Reliable Rehearsal toward Cellular Imaging, *ACS Appl. Mater. Interfaces*, 2016, **8**, 20583–20590.

87 X. Liu, J. Xu, Y. Lv, W. Wu, W. Liu and Y. Tang, An ATP-selective, lanthanide complex luminescent probe, *Dalton Trans.*, 2013, **42**, 9840–9846.

88 J. Sahoo, R. Arunachalam, P. S. Subramanian, E. Suresh, A. Valkonen, K. Rissanen and M. Albrecht, Coordinatively Unsaturated Lanthanide(iii) Helicates: Luminescence Sensors for Adenosine Monophosphate in Aqueous Media, *Angew. Chem., Int. Ed.*, 2016, **55**, 1–6.

89 R. Mailhot, T. Traviss-Pollard, R. Pal and S. J. Butler, Cationic Europium Complexes for Visualizing Fluctuations in Mitochondrial ATP Levels in Living Cells, *Chem. – Eur. J.*, 2018, **24**, 10745–10755.

90 (*a*) Y. Kurishita, T. Kohira, A. Ojida and I. Hamachi, Organelle-Localizable Fluorescent Chemosensors for Site-Specific Multicolor Imaging of Nucleoside Polyphosphate Dynamics in Living Cells, *J. Am. Chem. Soc.*, 2012, **134**, 18779–18789; (*b*) L. Wang, L. Yuan, X. Zeng, J. Peng, Y. Ni, J. C. Er, W. Xu, B. K. Agrawalla, D. Su, B. Kim and Y.-T. Chang, A Multisite-Binding Switchable Fluorescent Probe for Monitoring Mitochondrial ATP Level Fluctuation in Live Cells, *Angew. Chem., Int. Ed.*, 2016, **55**, 1773–1776.

91 (*a*) S. Dong, Y. Wang, Y. Zhao, X. Zhou and H. Zheng, La^{3+}/$La(OH)_3$ loaded magnetic cationic hydrogel composites for phosphate removal: Effect of lanthanum species and mechanistic study, *Water Res.*, 2017, **126**, 433–441; (*b*) E. S. Dragan, D. Humelnicu and M. V. Dinu, Development of Chitosan-Poly(ethyleneimine) Based Double Network Cryogels and Their Application as Superadsorbents for Phosphate, *Carbohydr. Polym.*, 2019, **210**, 17–25.

92 (*a*) M. H. Hassan, R. Stanton, J. Secora, D. J. Trivedi and S. Andreescu, Ultrafast Removal of Phosphate from Eutrophic Waters Using a Cerium-Based Metal–Organic Framework, *ACS Appl. Mater. Interfaces*, 2020, **12**, 52788–52796; (*b*) S. Mazloomi, M. Yousefi, H. Nourmoradi and M. Shams, Evaluation of phosphate removal from aqueous solution using metal organic framework; isotherm, kinetic and thermodynamic study, *J. Environ. Health Sci. Eng.*, 2019, **17**, 209–218; (*c*) Y. Zhang, S. Sheng, S. Mao, X. Wu, Z. Li, W. Tao and I. R. Jenkinson, Highly sensitive and selective fluorescent detection of phosphate in water environment by a functionalized coordination polymer, *Water Res.*, 2019, **163**, 114883; (*d*) Q. Xie, Y. Li, Z. Lv, H. Zhou, X. Yang, J. Chen and H. Guo, Effective Adsorption and Removal of Phosphate from Aqueous Solutions and Eutrophic Water by Fe-based MOFs of MIL-101, *Sci. Rep.*, 2017, **7**, 3316.

93 (*a*) W. Huang, Y. Zhang and D. Li, Adsorptive removal of phosphate from water using mesoporous materials: A review, *J. Environ. Manage.*, 2017, **193**, 470–482; (*b*) H. Bacelo, A. M. A. Pintor, S. C. R. Santos, R. A. R. Boaventura and C. M. S. Botelho, Performance and prospects of different adsorbents for phosphorus uptake and recovery from water, *Chem. Eng. J.*, 2020, **381**, 122566.

94 (*a*) S. Morab, K. Chhodena, P. Negia and K. Ravindra, Utilization of Nano-Alumina and Activated Charcoal for Phosphate Removal from Wastewater, *Environ. Nanotechnol. Monit. Manage.*, 2017, **7**, 15–23; (*b*) D. Yadav, P. Kumar, M. Kapur and M. K. Mondal, Phosphate removal from aqueous solutions by nano–alumina for the effective remediation of eutrophication, *Environ. Prog. Sustainable Energy*, 2019, **38**, S77–S85.

95 (*a*) B. Wu, J. Wan, Y. Zhang, B. Pan and I. M. C. Lo, Selective Phosphate Removal from Water and Wastewater using Sorption: Process Fundamentals and Removal Mechanisms, *Environ. Sci. Technol.*, 2020, **54**, 50–66; (*b*) H. H. Nodeh, H. Sereshti, E. Z. Afsharian and N. Nouri, Enhanced removal of phosphate and nitrate ions from aqueous media using nanosized lanthanum hydrous doped on magnetic graphene nanocomposite, *J. Environ. Manage.*, 2017, **197**, 265–274.